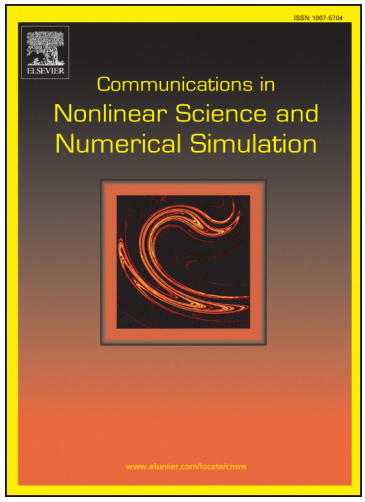

Homoclinic Solutions and Motion Chaotization in Attitude Dynamics of a Multi-Spin Spacecraft

Anton V. Doroshin

PII: S1007-5704(13)00526-1
DOI: http://dx.doi.org/10.1016/j.cnsns.2013.09.043
Reference: CNSNS 3002

To appear in: *Communications in Nonlinear Science and Numerical Simulation*

Received Date: 21 February 2013
Revised Date: 19 July 2013
Accepted Date: 2 September 2013

Please cite this article as: Doroshin, A.V., Homoclinic Solutions and Motion Chaotization in Attitude Dynamics of a Multi-Spin Spacecraft, *Communications in Nonlinear Science and Numerical Simulation* (2013), doi: http://dx.doi.org/10.1016/j.cnsns.2013.09.043

Homoclinic Solutions and Motion Chaotization in Attitude Dynamics of a Multi-Spin Spacecraft

Anton V. Doroshin

Space Engineering Department (Division of Flight Dynamics and Control Systems),
Samara State Aerospace University (National Research University),
SSAU, 34, Moskovskoe Shosse str., Samara, 443086, Russia

Abstract. The attitude dynamics of the multi-spin spacecraft (MSSC) and the torque-free angular motion of the multi-rotor system are considered. Some types of homoclinic and general solutions are obtained in hyperbolic and elliptic functions. The local homoclinic chaos in the MSSC angular motion is investigated under the influence of polyharmonic perturbations. Some possible applications of the multi-rotor system are indicated, including gyrostat-satellites, dual-spin spacecraft, roll-walking robots, and also the inertialess method of the spacecraft attitude (angular) reorientation/control.

Keywords: Multi-Rotor System, Multi-Spin Spacecraft, Dual-spin Spacecraft, Gyrostat, Exact Solutions, Homoclinic Chaos, Polyharmonic Perturbations, Melnikov Function, Poincaré Map, Roll-Walking Robot.

Introduction

The fundamental problem of the rigid body angular motion and corresponding applied tasks of the space flight mechanics and especially a spacecraft attitude dynamics remain very important and attract the attention of many scientists. The classical results in the framework of the indicated problem are described in [1-7] and in other well-known treatises. The modern research directions include many aspects [8-45]: the analytical/numerical modeling, the analysis/synthesis of the regular/chaotic motion of multi-body systems/spacecraft/vehicles with the constant/variable structure under the influence of perturbations. Here as parts of the problem we can indicate the comprehensive investigation of the attitude motion of a dual-spin spacecraft and gyrostats [8-17], the analysis/synthesis of the multi-rotor systems/spacecraft/vehicles dynamics [18-21], the general/homoclinic/heteroclinic solutions obtaining [22-31], the local/global chaos exploration [35-45].

First of all, we should indicate the dual-spin spacecraft (DSSC) and gyrostat-satellites (GS) as the important space-flight mechanics' application of the multi-body systems. The two-body construction of the DSSC allows fulfill the gyroscopic attitude stabilization with the help of the rotation of only one of the DSSC's bodies (the «rotor»-body) at the «quiescence» of the second body (the «platform»-body). The GS also contains the rotating rotors (usually one or three) for the creation of the gyrostatic momentum, and, moreover, the relative angular velocities of its rotors (with respect to the main GS' body) are constant. The investigation of various aspects of the DSSC/GS attitude dynamics is the urgent task which is considered in different formulations, e.g. [8-17].

As the further generalization of the GS construction we can present a multi-rotor (multi-spin) spacecraft. So, the multi-spin spacecraft (MSSC) is constructed as the multi-rotor system with conjugated pairs of rotors placed on the all inertia principle axes of the main body (fig.1). General properties of the MSSC motion are connected with the internal multi-rotor system (the multi-rotor kernel). This «spider»-type multi-rotor system was described in [18-21] where the attitude dynamics, spatial (attitude) reorientations of the MSSC and also roll-walking motions of multi-rotor robots are considered. The multi-rotor kernel allows to perform the attitude gyroscopic stabilization of the MSSC with the help of a compound spinup of the rotors. Also we

can use the MSSC in the traditional DSSC/GS-regimes. One of the important features of the MSSC is numerous independent internal degrees of freedom corresponding to the rotors' rotations. It is the powerful instrument for the spacecraft's attitude control and/or the angular reorientation with the help of an internal redistribution of the system angular momentum between the rotors and the main body.

For the purposes of the synthesis of necessary (in the framework of space missions) regimes of the DSSC/GS/MSSC attitude dynamics we need, first of all, to obtain the essential solutions and to analyze the properties of the torque-free angular motion of the corresponding mechanical systems – coaxial bodies, gyrostats and multi-rotor systems. These important solutions for DSSC/GS motion were obtained in different formulations in the papers [22-31]. The mentioned articles include the general and particular (homo/heteroclinic) solutions which can be used for the study of the SC weakly perturbed motion under the influence of external/internal disturbances (the gravitation/magnetic influence, the resistant environment, the construction asymmetry, etc.).

Here we have to note the importance of the indicated homo/heteroclinic solutions for the investigation of the local chaotic motion with the help of V.K.Melnikov's [35], S.Wiggins' [36] and P.J.Holmes'-J.E.Marsden's [37] approaches. The research results for the chaotic DSSC/GS motion analysis were presented, for example, in the papers [29-31, 38-41]. Also the study of the non-regular motion modes or, on the contrary, the study of the regularization/synchronization properties can be performed with the help of the special methods [42-45].

So, in this paper the MSSC attitude dynamics is considered, some homoclinic and general exact solutions are obtained, and cases of chaotic and regular motion under the influence of polyharmonic disturbances are investigated.

1. Mechanical and mathematical models of the system

Let us investigate the torque-free attitude dynamics of the MSSC and the angular motion of the multi-rotor mechanical system (Fig.1) about its mass center (the "fixed" point O).

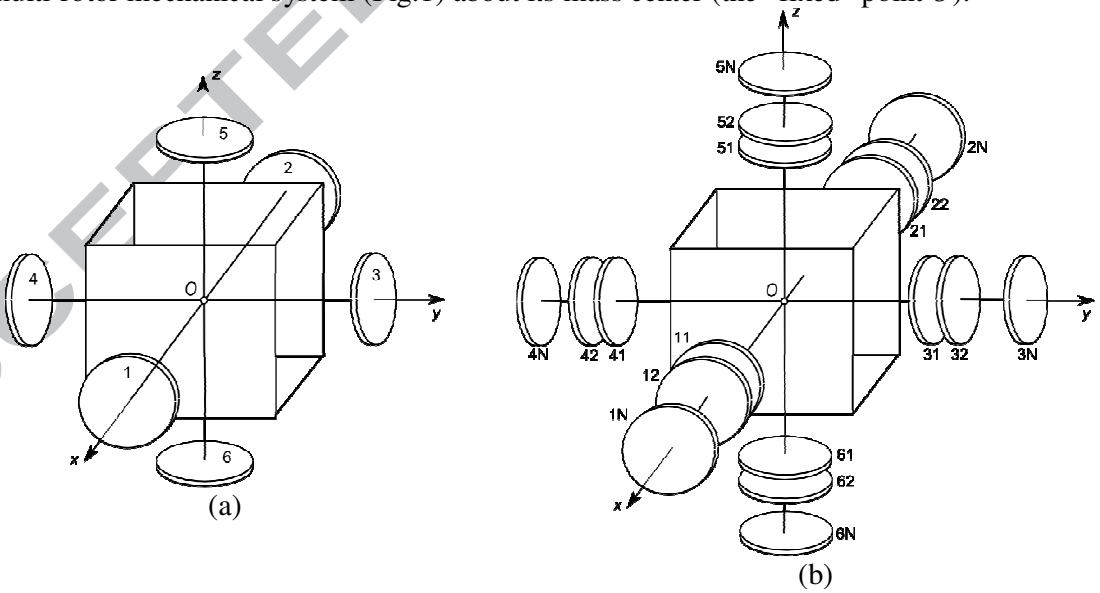

Fig. 1. The multi-rotor systems (the multi-spin spacecraft)

First of all, we need to consider the multi-rotor system with six identical rotors symmetrically placed on the general axes of the main body (Fig.1-a). Then the angular momentum of the system can be written in projections onto the frame $Oxyz$ axes connected with the central main body

$$\mathbf{K} = \mathbf{K}_m + \mathbf{K}_r \tag{1.1}$$

$$\mathbf{K}_m = \begin{bmatrix} \tilde{A}p \\ \tilde{B}q \\ \tilde{C}r \end{bmatrix} + (4J + 2I)\begin{bmatrix} p \\ q \\ r \end{bmatrix}, \quad \mathbf{K}_r = I\begin{bmatrix} \sigma_1 + \sigma_2 \\ \sigma_3 + \sigma_4 \\ \sigma_5 + \sigma_6 \end{bmatrix} \tag{1.2}$$

where $\mathbf{K}_m$ is the angular momentum of the main body with the fixed ("frozen") rotors; $\mathbf{K}_r$ is the relative angular momentum of the rotors; $\boldsymbol{\omega}=[p,\ q,\ r]^{\mathrm{T}}$ – the vector of the absolute angular velocity of the main body; σ_i - the relative angular velocity of the i-th rotor; $\tilde{A}$, $\tilde{B}$, $\tilde{C}$ are the general moments of inertia of the main body; I is the longitudinal inertia moment of the rotor; J is the equatorial inertia moment of the rotor calculated relatively the point O.

The angular motion equations of the system can be written with the help of the law of the angular momentum's variation in the moving coordinates frame $Oxyz$

$$\frac{d\mathbf{K}}{dt} + \boldsymbol{\omega} \times \mathbf{K} = \mathbf{M}^e \tag{1.3}$$

where $\mathbf{M}^e$ is the external torque. The vector equation (1.3) can be rewritten

$$\begin{cases} A\dot{p} + I\dot{\sigma}_{12} + (C - B)qr + I(q\sigma_{56} - r\sigma_{34}) = M_x^e \\ B\dot{q} + I\dot{\sigma}_{34} + (A - C)pr + I(r\sigma_{12} - p\sigma_{56}) = M_y^e \\ C\dot{r} + I\dot{\sigma}_{56} + (B - A)pq + I(p\sigma_{34} - q\sigma_{12}) = M_z^e \end{cases} \tag{1.4}$$

where

$$\begin{aligned} &\sigma_{ij} = \sigma_i + \sigma_j, \qquad A = \tilde{A} + 4J + 2I \\ &B = \tilde{B} + 4J + 2I, \quad C = \tilde{C} + 4J + 2I \end{aligned} \tag{1.5}$$

The rotors' relative motion equations are written in the form

$$\begin{cases} I(\dot{p} + \dot{\sigma}_1) = M_1^i + M_{1x}^e; \ I(\dot{p} + \dot{\sigma}_2) = M_2^i + M_{2x}^e \\ I(\dot{q} + \dot{\sigma}_3) = M_3^i + M_{3y}^e; \ I(\dot{q} + \dot{\sigma}_4) = M_4^i + M_{4y}^e \\ I(\dot{r} + \dot{\sigma}_5) = M_5^i + M_{5z}^e; \ I(\dot{r} + \dot{\sigma}_6) = M_6^i + M_{6z}^e \end{cases} \tag{1.6}$$

where M_j^i is the torque of the internal forces acting between the main body and the j-th rotor; M_{jx}^e, M_{jy}^e, M_{jz}^e are the torques from the external forces acting only on the j-th rotor.

The equations (1.4) and (1.6) form the complete dynamical system.

We can generalize the dynamical equations for the multi-rotor system with $6N$ rotors (Fig.1-b). This system contains N layers with rotors on the six general directions coinciding with the principle axes of the main body. We also assume that each layer contains the equal rotors, but the rotors in the different layers are different. For the angular momentum of the generalized $6N$-rotors-system we have

$$\begin{aligned} &\mathbf{K}_m = \begin{bmatrix} Ap \\ Bq \\ Cr \end{bmatrix}; \quad \mathbf{K}_r = \sum_{l=1}^{N} I_l \begin{bmatrix} \sigma_{1l} + \sigma_{2l} \\ \sigma_{3l} + \sigma_{4l} \\ \sigma_{5l} + \sigma_{6l} \end{bmatrix}; \\ &A = \tilde{A} + 4\bar{J} + 2\bar{I}, \quad B = \tilde{B} + 4\bar{J} + 2\bar{I}, \quad C = \tilde{C} + 4\bar{J} + 2\bar{I}; \\ &\bar{J} = \sum_{l=1}^{N} J_l; \qquad \bar{I} = \sum_{l=1}^{N} I_l; \end{aligned} \tag{1.7}$$

Here σ_{kl} is the relative angular velocity of the *kl*-th rotor (relatively the main body); I_l and J_l are the longitudinal and the equatorial inertia moments of the *l*-layer-rotor relatively the point *O*.

Then the equation (1.3) can be written in the following scalar form

$$\begin{cases} A\dot{p}+\sum_{l=1}^{N} I_l\left(\dot{\sigma}_{1l}+\dot{\sigma}_{2l}\right)+\left(C-B\right)qr+\left[q\sum_{l=1}^{N} I_l\left(\sigma_{5l}+\sigma_{6l}\right)-r\sum_{l=1}^{N} I_l\left(\sigma_{3l}+\sigma_{4l}\right)\right]=M_x^e \\ B\dot{q}+\sum_{l=1}^{N} I_l\left(\dot{\sigma}_{3l}+\dot{\sigma}_{4l}\right)+\left(A-C\right)pr+\left[r\sum_{l=1}^{N} I_l\left(\sigma_{1l}+\sigma_{2l}\right)-p\sum_{l=1}^{N} I_l\left(\sigma_{5l}+\sigma_{6l}\right)\right]=M_y^e \\ C\dot{r}+\sum_{l=1}^{N} I_l\left(\dot{\sigma}_{5l}+\dot{\sigma}_{6l}\right)+\left(A-C\right)qp+\left[p\sum_{l=1}^{N} I_l\left(\sigma_{3l}+\sigma_{4l}\right)-q\sum_{l=1}^{N} I_l\left(\sigma_{1l}+\sigma_{2l}\right)\right]=M_z^e \end{cases} \quad (1.8)$$

The relative motion equations of the rotors are $\left(l=1..N\right)$

$$\begin{cases} I_l\left(\dot{p}+\dot{\sigma}_{1l}\right)=M_{1l}^i+M_{1lx}^e;\;\; I_l\left(\dot{p}+\dot{\sigma}_{2l}\right)=M_{2l}^i+M_{2lx}^e \\ I_l\left(\dot{q}+\dot{\sigma}_{3l}\right)=M_{3l}^i+M_{3ly}^e;\;\; I_l\left(\dot{q}+\dot{\sigma}_{4l}\right)=M_{4l}^i+M_{4ly}^e \\ I_l\left(\dot{r}+\dot{\sigma}_{5l}\right)=M_{5l}^i+M_{5lz}^e;\;\; I_l\left(\dot{r}+\dot{\sigma}_{6l}\right)=M_{6l}^i+M_{6lz}^e \end{cases} \quad (1.9)$$

The equation system (1.8) with *N* systems (1.9) completely describe the angular motion of the multi-rotor system with 6*N* rotors and the attitude dynamics of the multi-spin spacecraft (Fig.1-b).

2. The Hamiltonian form of the motion equations

Now we construct the mathematical model of the *N*-layers-multi-rotor system's motion in the Hamiltonian form.

The kinetic energy expressions for the six rotors in the *j*-layer are

$$\begin{aligned} &2T_{1j}=J_j\left(q^2+r^2\right)+I_j\left(p+\sigma_{1j}\right)^2;\;\; 2T_{2j}=J_j\left(q^2+r^2\right)+I_j\left(p+\sigma_{2j}\right)^2 \\ &2T_{3j}=J_j\left(p^2+r^2\right)+I_j\left(q+\sigma_{3j}\right)^2;\;\; 2T_{4j}=J_j\left(p^2+r^2\right)+I_j\left(q+\sigma_{4j}\right)^2 \\ &2T_{5j}=J_j\left(p^2+q^2\right)+I_j\left(r+\sigma_{5j}\right)^2;\;\; 2T_{6j}=J_j\left(p^2+q^2\right)+I_j\left(r+\sigma_{6j}\right)^2 \end{aligned} \quad (2.1)$$

Then the full system's kinetic energy is equal to

$$\begin{aligned} &T=T_0+\sum_{j=1}^{N} T_j;\quad 2T_0=\tilde{A}p^2+\tilde{B}q^2+\tilde{C}r^2;\quad T_j=\sum_{i=1}^{6} T_{ij}; \\ &2T_j=\left(2I_j+4J_j\right)\left(p^2+q^2+r^2\right)+ \\ &+2I_j\left(p\left[\sigma_{1j}+\sigma_{2j}\right]+q\left[\sigma_{3j}+\sigma_{4j}\right]+r\left[\sigma_{5j}+\sigma_{6j}\right]\right)+I_j\sum_{i=1}^{6}\sigma_{ij}^2 \end{aligned} \quad (2.2)$$

In purposes of the Hamiltonian formalism application we introduce the well-known Andoyer-Deprit canonical variables [6, 7]. With the help of these variables the angular motion of the system's main body is described by the angles $\left(\varphi_3,\, \varphi_2,\, l\right)$ of the rotations about the axis *OZ*, about the angular momentum direction, and about the axis Oz (Fig.2). The canonical Andoyer-Deprit momentums are defined by the following expressions

$$L=\frac{\partial \mathrm{T}}{\partial \dot{l}}=\mathbf{K}\cdot\mathbf{k},\quad G=\frac{\partial \mathrm{T}}{\partial \dot{\varphi}_2}=\mathbf{K}\cdot\mathbf{s}=K,\quad H=\frac{\partial \mathrm{T}}{\partial \dot{\varphi}_3}=\mathbf{K}\cdot\mathbf{k}',\quad \Delta_{ij}=\frac{\partial \mathrm{T}}{\partial \dot{\delta}_{ij}}=\frac{\partial \mathrm{T}}{\partial \sigma_{ij}} \quad (2.3)$$

where δ_{ij} is the relative rotation angle of the *ij*-rotor $\left(\dot{\delta}_{ij}=\sigma_{ij}\right)$.

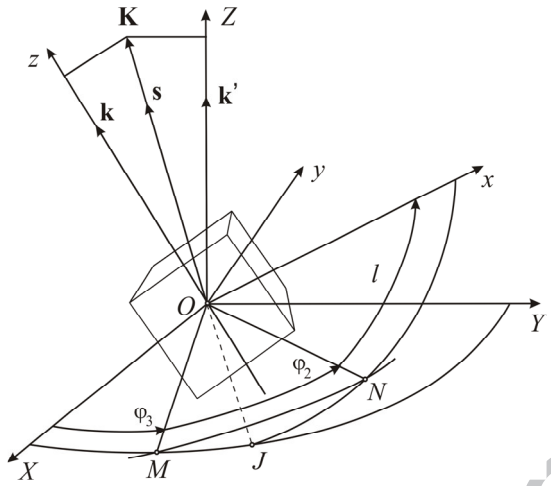

Fig. 2. The Andoyer-Deprit variables and the system's main body frame

The components of the system angular momentum can be expressed as the functions of the Andoyer-Deprit variables:

$$K_x = \sqrt{G^2 - L^2}\,\sin l = Ap + \sum_{j=1}^{N} I_j\left(\sigma_{1j} + \sigma_{2j}\right)$$

$$K_y = \sqrt{G^2 - L^2}\,\cos l = Bq + \sum_{j=1}^{N} I_j\left(\sigma_{3j} + \sigma_{4j}\right) \tag{2.4}$$

$$K_z = L = Cr + \sum_{j=1}^{N} I_j\left(\sigma_{5j} + \sigma_{6j}\right), \qquad \left(L \le G\right)$$

The canonical momentums for the relative motion of the *j*-layer-rotors are

$$\begin{aligned} &\Delta_{1j} = I_j\left(p + \sigma_{1j}\right); \quad \Delta_{2j} = I_j\left(p + \sigma_{2j}\right) \\ &\Delta_{3j} = I_j\left(q + \sigma_{3j}\right); \quad \Delta_{4j} = I_j\left(q + \sigma_{4j}\right) \\ &\Delta_{5j} = I_j\left(r + \sigma_{5j}\right); \quad \Delta_{6j} = I_j\left(r + \sigma_{6j}\right) \end{aligned} \tag{2.5}$$

From (2.5) the expressions follow

$$\sum_{j=1}^{N} I_j\left(\sigma_{1j} + \sigma_{2j}\right) = \sum_{j=1}^{N}\left(\Delta_{1j} + \Delta_{2j}\right) - 2p\sum_{j=1}^{N} I_j \tag{2.6}$$

$$\sum_{j=1}^{N} I_j\left(\sigma_{3j} + \sigma_{4j}\right) = \sum_{j=1}^{N}\left(\Delta_{3j} + \Delta_{4j}\right) - 2q\sum_{j=1}^{N} I_j \tag{2.7}$$

$$\sum_{j=1}^{N} I_j\left(\sigma_{5j} + \sigma_{6j}\right) = \sum_{j=1}^{N}\left(\Delta_{5j} + \Delta_{6j}\right) - 2r\sum_{j=1}^{N} I_j \tag{2.8}$$

Using the expressions (2.5)-(2.8) the components of the main body angular velocity can be written

$$p = \frac{1}{\hat{A}}\left[\sqrt{G^2 - L^2}\,\sin l - \sum_{j=1}^{N}\left(\Delta_{1j} + \Delta_{2j}\right)\right] \tag{2.9}$$

$$q=\frac{1}{\hat{B}}\left[\sqrt{G^2-L^2}\cos l-\sum_{j=1}^{N}\left(\Delta_{3j}+\Delta_{4j}\right)\right] \tag{2.10}$$

$$r=\frac{1}{\hat{C}}\left[L-\sum_{j=1}^{N}\left(\Delta_{5j}+\Delta_{6j}\right)\right] \tag{2.11}$$

where $\hat{A}=A-2\sum_{j=1}^{N}I_j;\ \hat{B}=B-2\sum_{j=1}^{N}I_j;\ \hat{C}=C-2\sum_{j=1}^{N}I_j$.

Also we can rewrite the system's kinetic energy and the angular momentum's components:

$$\begin{cases} T=T_0+\sum_{j=1}^{N}T_j;\quad 2T_0=\tilde{A}p^2+\tilde{B}q^2+\tilde{C}r^2;\quad T_j=\sum_{i=1}^{6}T_{ij};\\ 2T_{1j}=J_j\left(q^2+r^2\right)+\frac{\Delta_{1j}^2}{I_j};\quad 2T_{2j}=J_j\left(q^2+r^2\right)+\frac{\Delta_{2j}^2}{I_j};\\ 2T_{3j}=J_j\left(p^2+r^2\right)+\frac{\Delta_{3j}^2}{I_j};\quad 2T_{4j}=J_j\left(p^2+r^2\right)+\frac{\Delta_{4j}^2}{I_j};\\ 2T_{5j}=J_j\left(p^2+q^2\right)+\frac{\Delta_{5j}^2}{I_j};\quad 2T_{6j}=J_j\left(p^2+q^2\right)+\frac{\Delta_{6j}^2}{I_j};\\ 2T_j=4J_j\left(p^2+q^2+r^2\right)+\frac{1}{I_j}\sum_{i=1}^{6}\Delta_{ij}^2;\\ 2\sum_{j=1}^{N}T_j=\left(p^2+q^2+r^2\right)\sum_{j=1}^{N}\left(4J_j\right)+\sum_{j=1}^{N}\sum_{i=1}^{6}\frac{\Delta_{ij}^2}{I_j}; \end{cases} \tag{2.12}$$

$$2T=\hat{A}p^2+\hat{B}q^2+\hat{C}r^2+2T_R;\quad T_R=\frac{1}{2}\sum_{j=1}^{N}\sum_{i=1}^{6}\frac{\Delta_{ij}^2}{I_j}; \tag{2.13}$$

$$\begin{aligned} K_x&=\hat{A}p+\sum_{j=1}^{N}\left(\Delta_{1j}+\Delta_{2j}\right)=\hat{A}p+D_{12};\\ K_y&=\hat{B}q+\sum_{j=1}^{N}\left(\Delta_{3j}+\Delta_{4j}\right)=\hat{B}q+D_{34};\\ K_z&=\hat{C}r+\sum_{j=1}^{N}\left(\Delta_{5j}+\Delta_{6j}\right)=\hat{C}r+D_{56}; \end{aligned} \tag{2.14}$$

$$K^2=\left(\hat{A}p+D_{12}\right)^2+\left(\hat{B}q+D_{34}\right)^2+\left(\hat{C}r+D_{56}\right)^2, \tag{2.15}$$

where D_{nm} are the following axial summarized angular momentums of the rotors:

$$D_{12}=\sum_{j=1}^{N}\left[\Delta_{1j}+\Delta_{2j}\right],\quad D_{34}=\sum_{j=1}^{N}\left[\Delta_{3j}+\Delta_{4j}\right],\quad D_{56}=\sum_{j=1}^{N}\left[\Delta_{5j}+\Delta_{6j}\right] \tag{2.16}$$

Taking into account the expressions (2.16), (2.6)-(2.8), the main dynamical equations (1.8) are rewritten in the unbalanced-gyrostat-form

$$\begin{cases} \hat{A}\dot{p}+\dot{D}_{12}+\left(\hat{C}-\hat{B}\right)qr+\left[qD_{56}-rD_{34}\right]=M_x^e \\ \hat{B}\dot{q}+\dot{D}_{34}+\left(\hat{A}-\hat{C}\right)rp+\left[rD_{12}-pD_{56}\right]=M_y^e \\ \hat{C}\dot{r}+\dot{D}_{56}+\left(\hat{B}-\hat{A}\right)pq+\left[pD_{34}-qD_{12}\right]=M_z^e \end{cases} \tag{2.17}$$

Based on (1.9) we obtain the equations for the rotors' summarized angular momentums (2.16):

$$\dot{D}_{12}=M_{12}^i+M_{12}^e; \quad \dot{D}_{34}=M_{34}^i+M_{34}^e; \quad \dot{D}_{56}=M_{56}^i+M_{56}^e, \tag{2.18}$$

where

$$M_{12}^i=\sum_{l=1}^{N}\left(M_{1l}^i+M_{2l}^i\right), \quad M_{12}^e=\sum_{l=1}^{N}\left(M_{1lx}^e+M_{2lx}^e\right)$$
$$M_{34}^i=\sum_{l=1}^{N}\left(M_{3l}^i+M_{4l}^i\right), \quad M_{34}^e=\sum_{l=1}^{N}\left(M_{3ly}^e+M_{4ly}^e\right)$$
$$M_{56}^i=\sum_{l=1}^{N}\left(M_{5l}^i+M_{6l}^i\right), \quad M_{56}^e=\sum_{l=1}^{N}\left(M_{5lz}^e+M_{6lz}^e\right)$$

With the help of (2.9)-(2.11) we express the system kinetic energy (2.2) as the function of the Andoyer-Deprit variables:

$$2T=\left(G^2-L^2\right)\left[\frac{\sin^2 l}{\hat{A}}+\frac{\cos^2 l}{\hat{B}}\right]+\frac{1}{\hat{C}}\left(L-\sum_{j=1}^{N}\left[\Delta_{5j}+\Delta_{6j}\right]\right)^2-$$
$$-2\sqrt{G^2-L^2}\left\{\frac{\sin l}{\hat{A}}\cdot\sum_{j=1}^{N}\left[\Delta_{1j}+\Delta_{2j}\right]+\frac{\cos l}{\hat{B}}\cdot\sum_{j=1}^{N}\left[\Delta_{3j}+\Delta_{4j}\right]\right\}+ \tag{2.19}$$
$$+\frac{1}{\hat{A}}\left(\sum_{j=1}^{N}\left[\Delta_{1j}+\Delta_{2j}\right]\right)^2+\frac{1}{\hat{B}}\left(\sum_{j=1}^{N}\left[\Delta_{3j}+\Delta_{4j}\right]\right)^2+\sum_{j=1}^{N}\sum_{i=1}^{6}\frac{\Delta_{ij}^2}{I_j}$$

The Hamiltonian and canonical equations have the form (P – the system potential energy)

$$H=T+P=\frac{G^2-L^2}{2}\left[\frac{\sin^2 l}{\hat{A}}+\frac{\cos^2 l}{\hat{B}}\right]+\frac{1}{2\hat{C}}\left(L-D_{56}\right)^2-$$
$$-\sqrt{G^2-L^2}\left\{\frac{D_{12}\sin l}{\hat{A}}+\frac{D_{34}\cos l}{\hat{B}}\right\}+\frac{D_{12}^2}{2\hat{A}}+\frac{D_{34}^2}{2\hat{B}}+\frac{1}{2}\sum_{j=1}^{N}\sum_{i=1}^{6}\frac{\Delta_{ij}^2}{I_j}+P\left(l,\varphi_2,\varphi_3,\delta_{ij}\right); \tag{2.20}$$
$$D_{12}=\sum_{j=1}^{N}\left[\Delta_{1j}+\Delta_{2j}\right], \quad D_{34}=\sum_{j=1}^{N}\left[\Delta_{3j}+\Delta_{4j}\right], \quad D_{56}=\sum_{j=1}^{N}\left[\Delta_{5j}+\Delta_{6j}\right];$$

$$\dot{x}=\frac{\partial H}{\partial X}; \quad \dot{X}=-\frac{\partial H}{\partial x} \tag{2.21}$$
$$x=\left\{l,\varphi_2,\varphi_3,\delta_{ij}\right\}, \quad X=\left\{L,G,H,\Delta_{ij}\right\}$$

In the case of the absence of internal/external forces and torques (P=0) the system's kinetic energy and the angular momentum are constant

$$T=E=\text{const}; \quad K=G=\text{const} \tag{2.22}$$

Here we can to note, that the expression (2.20) is the important generalization of the Hamiltonian's form corresponded to the task of the one-rotor-gyrostat's angular motion [14, 24-28].

3. The system phase portraits and the homoclinic orbits

Let's investigate the system torque-free motion $\left(M_x^e = M_y^e = M_z^e = M_{ij}^e = 0\right)$ and obtain the exact solutions for the homoclinic phase trajectories in the three-dimensional space corresponding to the angular velocities components (or in the topologically equivalent space of the angular momentum components). In this research we assume

$$\hat{A} \le \hat{B} < \hat{C}; \quad D_{12} = D_{56} = 0; \quad D_{34} = \text{const} > 0. \tag{2.23}$$

Here we note that the assumption (2.23) is valid for the realization of the symmetrical spinup of the rotors on the rays 1-2 and 5-6 (fig.1). Therefore the total values of the summarized angular momentums of these rotors are equal to zero $\left(D_{12} = D_{56} = 0\right)$. The equatorial axis *Oy* (the intermediate inertia axis) contains the rotors with the nonzero total angular momentum D_{34}.

3.1. The case of the dynamical symmetry of the main body

First of all let's consider the angular motion of the system with the dynamical symmetry of the main body $\left(\hat{A} = \hat{B}\right)$.

In this case we have the following structure of the polhodes on the ellipsoid of the angular momentum (fig.3)[1] [e.g., 2, 24, 27, 28, 31]. This structure has one homoclinic trajectory (the homoclinic polhode) with the saddle point $S\left(p = 0,\ q = q_* > 0,\ r = 0\right)$ and with two loops (blue line). Also we need to note that in the considering case the following inequality takes place along the homoclinic trajectory:

$$\forall t \in \left(-\infty, +\infty\right):\ q\left(t\right) \le q_* \tag{2.24}$$

The constants (2.22) for the homoclinic trajectory (at the arbitrary value q_*) are equal to

$$2E = 2E_* = \hat{A}q_*^2 + 2T_R; \qquad K^2 = K_*^2 = \left(\hat{A}q_* + D_{34}\right)^2 \tag{2.25}$$

Now we can write the dependences for the homoclinic polhode with the help of the combination of expressions (2.15), (2.13) ((2.13) with the multiplier $\hat{A}$) and (2.25) [28, 31]

$$\begin{gathered} \hat{C}\left(\hat{C} - \hat{A}\right)r^2 + 2\hat{A}D_{34}q = P; \\ P = K_*^2 - 2\hat{A}E_* + 2\hat{A}T_R - D_{34}^2 = 2\hat{A}q_*D_{34} \end{gathered} \tag{2.26}$$

From (2.26) the parabola's dependence follows (for the corresponding curves on the *Oqr*-projection)

$$\begin{gathered} q_* - q = \frac{\hat{C}\left(\hat{C} - \hat{A}\right)}{2\hat{A}D_{34}}r^2 \\ r = \pm\sqrt{\frac{2\hat{A}D_{34}\left(q_* - q\right)}{\hat{C}\left(\hat{C} - \hat{A}\right)}} \end{gathered} \tag{2.27}$$

Using expressions (2.15), (2.13) ((2.13) with the multiplier $\hat{C}$) and the perfect square separating we can obtain:

[1] The numerical modeling (and the numerical results plotting) in the angular momentum (or in the angular velocity) components' space is performed based on the numerical integration of the equations (2.17) and (2.18).

$$\hat{A}\left(\hat{C}-\hat{A}\right)p^2+\left[\sqrt{\hat{A}\left(\hat{C}-\hat{A}\right)}q-\frac{D_{34}\sqrt{\hat{A}}}{\sqrt{\hat{C}-\hat{A}}}\right]^2=R;$$
$$R=\hat{C}\hat{A}q_*^2-\left(\hat{A}q_*+D_{34}\right)^2+D_{34}^2+\frac{\hat{A}}{\hat{C}-\hat{A}}D_{34}^2=\hat{A}\left(q_*\sqrt{\hat{C}-\hat{A}}-\frac{D_{34}}{\sqrt{\hat{C}-\hat{A}}}\right)^2 \tag{2.28}$$

From (2.28) the ellipse's equation follows (for the corresponding curves on the *Opq*-projection)

$$p=\pm\sqrt{\left[q_*-\frac{D_{34}}{\hat{C}-\hat{A}}\right]^2-\left[q-\frac{D_{34}}{\hat{C}-\hat{A}}\right]^2}=\pm\sqrt{\left(q_*+q-\frac{2D_{34}}{\hat{C}-\hat{A}}\right)\left(q_*-q\right)} \tag{2.29}$$

In the considered case the second equation (2.17) can be rewritten

$$\hat{A}\dot{q}=\left(\hat{C}-\hat{A}\right)pr \tag{2.30}$$

Here we can note that the following coordinates for the point *S* and the vertices $V_{1,2}$ (fig.3) take place

$$p\left(S\right)=0;\;\; q\left(S\right)=q_*$$
$$p(V_{1,2})=0;\;\; q(V_{1,2})=q_V=\frac{2D_{34}}{\hat{C}-\hat{A}}-q_*$$

Using (2.27) and (2.29) we rewrite the last equation (2.30) in the form

$$\hat{A}\dot{q}=\pm\left(\hat{C}-\hat{A}\right)\sqrt{\frac{2\hat{A}D_{34}}{\hat{C}\left(\hat{C}-\hat{A}\right)}}\sqrt{\left(q+q_*-\frac{2D_{34}}{\hat{C}-\hat{A}}\right)}\left(q_*-q\right) \tag{2.31}$$

The integration of (2.31) gives us

$$\int_{q_0}^{q}\frac{dq}{\sqrt{\left(q+q_*-\frac{2D_{34}}{\hat{C}-\hat{A}}\right)\left(q_*-q\right)}}=\pm\int_0^t Mdt;\quad M=\frac{\left(\hat{C}-\hat{A}\right)}{\hat{A}}\sqrt{\frac{2\hat{A}D_{34}}{\hat{C}\left(\hat{C}-\hat{A}\right)}} \tag{2.32}$$

where we can take the vertex $V_{1,2}$ as the start of the homoclinic trajectory with the corresponding initial *q*-value: $q\big|_{t=0}=q_0=q_V=\frac{2D_{34}}{\hat{C}-\hat{A}}-q_*$; then the saddle point *S* is the end of the homoclinic trajectory at $t\to\pm\infty$. The reduced form of the integral (2.32) can be written as follows

$$\int_{q_V}^{q}\frac{dq}{\sqrt{\left(q-q_*+b\right)\left(q-q_*\right)}}=\pm\int_0^t Mdt;$$
$$M=\sqrt{\frac{2\left(\hat{C}-\hat{A}\right)D_{34}}{\hat{A}\hat{C}}};\quad b=2q_*-\frac{2D_{34}}{\hat{C}-\hat{A}}>0 \tag{2.33}$$

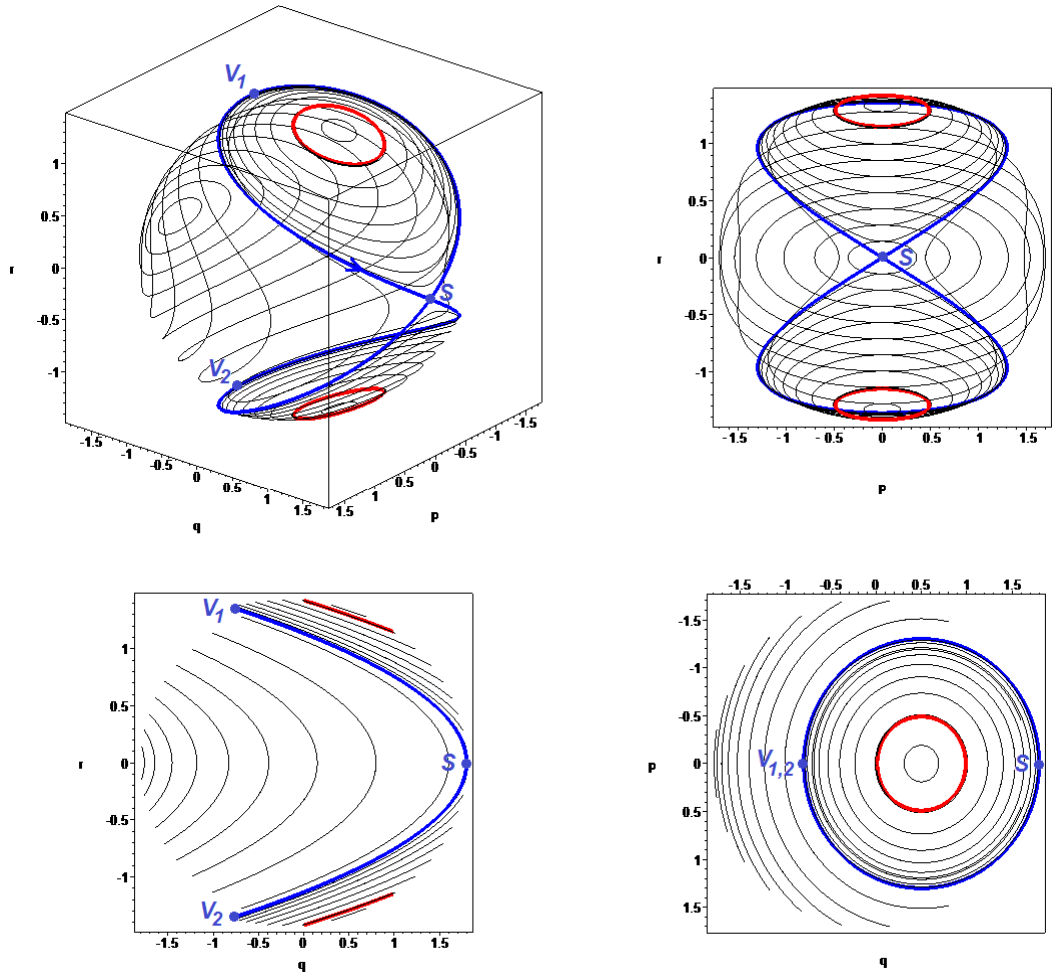

Fig.3 The angular momentum ellipsoid with the plane projections
A=0.5, B=0.5, C=0.7 [kg·m^2]; D_{34}=0.1, K_*=1 [kg·m^3/s]

The last integral can be evaluated with the help of the standard quadrature [33]

$$\int \frac{dx}{x\sqrt{(ax+b)}} = \frac{1}{\sqrt{b}} \ln \left| \frac{\sqrt{ax+b}-\sqrt{b}}{\sqrt{ax+b}+\sqrt{b}} \right|$$

As the result we obtain

$$\pm Mt = \frac{1}{\sqrt{b}} \ln \left| \frac{\sqrt{q-q_*+b}-\sqrt{b}}{\sqrt{q-q_*+b}+\sqrt{b}} \right|_{q_V}^{q} = \frac{1}{\sqrt{b}} \ln \left| \frac{\sqrt{q-q_*+b}-\sqrt{b}}{\sqrt{q-q_*+b}+\sqrt{b}} \right| \qquad (2.34)$$

Using (2.24) we can solve the problem with modules in (2.34):

$$\pm Mt = \frac{1}{\sqrt{b}} \ln \frac{\left(\sqrt{2q_* - \frac{2D_{34}}{\hat{C}-\hat{A}}} - \sqrt{q+q_* - \frac{2D_{34}}{\hat{C}-\hat{A}}} \right)}{\left(\sqrt{q+q_* - \frac{2D_{34}}{\hat{C}-\hat{A}}} + \sqrt{2q_* - \frac{2D_{34}}{\hat{C}-\hat{A}}} \right)} \qquad (2.35)$$

After some transformations the analytical dependences for the homoclinic polhode follow from (2.35):

$$q(t)=\left(2q_*-\frac{2D_{34}}{\hat{C}-\hat{A}}\right)\frac{\left(1-\exp\left(\pm\sqrt{b}Mt\right)\right)^2}{\left(\exp\left(\pm\sqrt{b}Mt\right)+1\right)^2}-q_*+\frac{2D_{34}}{\hat{C}-\hat{A}};\qquad(2.36)$$

$$p(t)=p\left(q(t)\right);\qquad r(t)=r\left(q(t)\right);$$

where the explicit homoclinic dependences $p(t)$ and $r(t)$ are obtained with the help of the substitution of the solution (2.36) into expressions (2.29) and (2.27). The verification (Fig.4) demonstrates the full coincidence of the analytical results (2.36) and the numerical calculations.

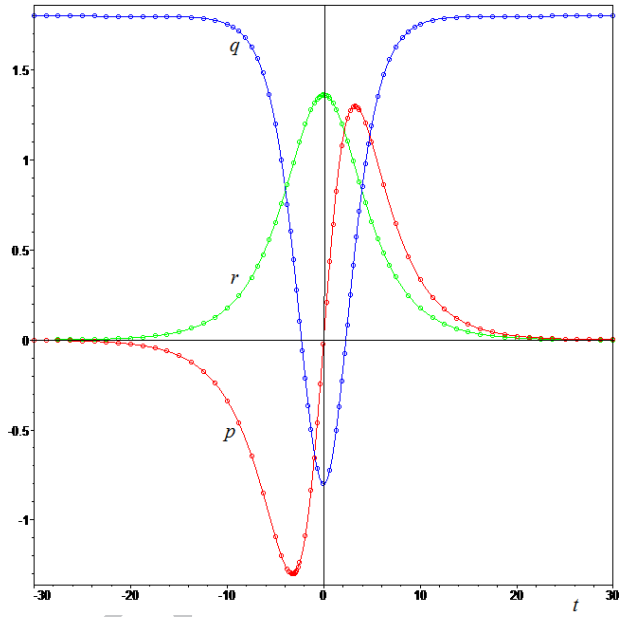

Fig.4 The homoclinic dependences:
the analytical results (points) and the numerical integrations (lines)
A=0.5, B=0.5, C=0.7 [kg·m^2]; D_{34}=0.1, K_*=1 [kg·m^2/s]

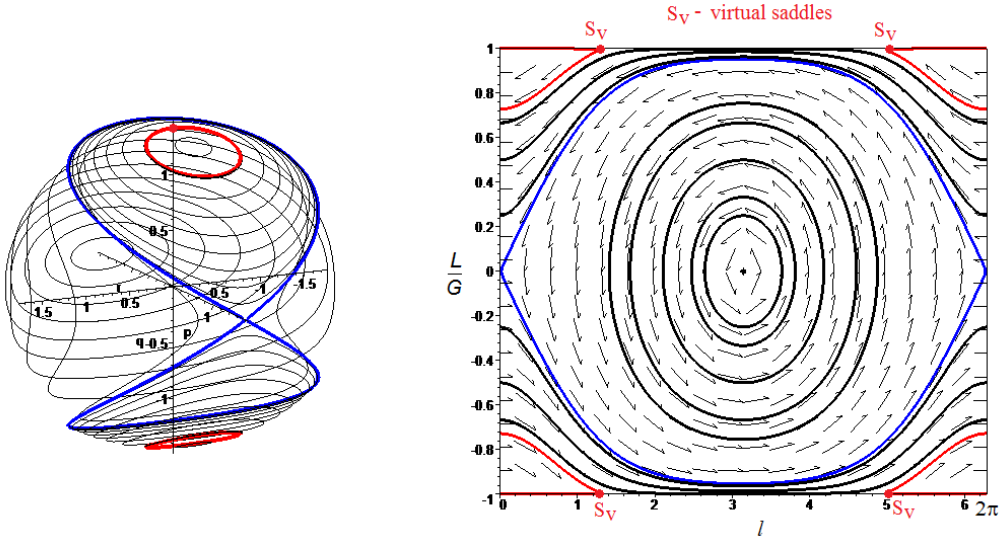

Fig.5 The correspondence between the angular momentum's ellipsoid and the Andoyer-Deprit phase space
A=0.5, B=0.5, C=0.7 [kg·m^2]; D_{34}=0.1, K_*=1 [kg·m^2/s]

As we can see (fig.5)[2] the Andoyer-Deprit phase space has the virtual heteroclinic phase trajectories (red lines) with the virtual saddles-points (S_V) connected with the following initial conditions

$$\{L(0)=\pm G=\pm K_*\}\Leftrightarrow\left\{r(0)=\pm\frac{\sqrt{K_*^2-D_{34}^2}}{\hat{C}};\,p(0)=q(0)=0\right\}$$

These virtual saddles points and the corresponding virtual heteroclinic trajectories vanish at the topological transformation of the Andoyer-Deprit plane to the angular momentum's spherical structure: in the angular momentum's space these phase trajectories correspond to the ordinary polhodes with the maximal absolute values of K_z-components $(|K_z|=K_*)$.

3.2. The case of the three-axial inertia tensor of the main body

Let's consider the motion of the system with the general inertia tensor of the main body $(\hat{A}<\hat{B}<\hat{C})$. Corresponding structures of the angular momentum ellipsoid [e.g., 2, 24, 27, 28, 31] and the Andoyer-Deprit phase space are presented at fig.6,7. We have two homoclinic two-loop orbits with the saddle points S_1, S_2 and the loop-vertex points $V_{1,2}$ and $W_{1,2}$.

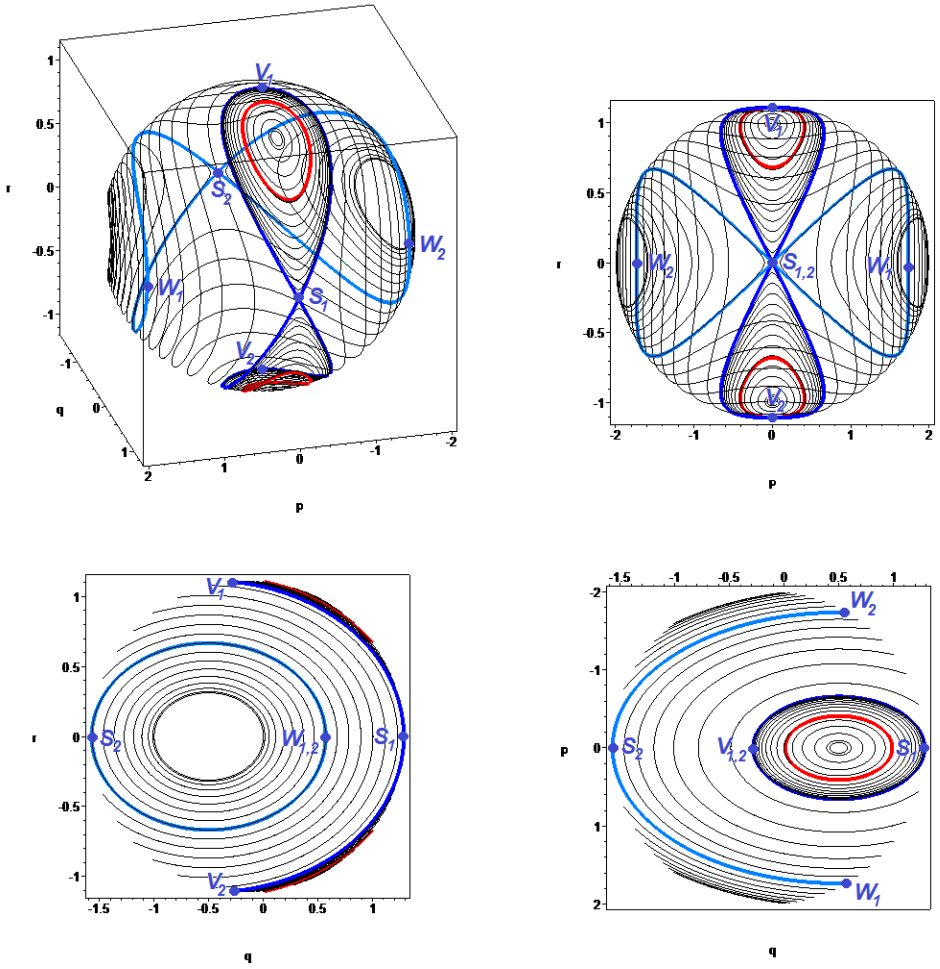

Fig.6 The angular momentum ellipsoid with the plane projections

A=0.5, B=0.7, C=0.9 [kg·m^2]; D_{34}=0.1, K_*=1 [kg·m^2/s]

[2] The numerical modeling (and the numerical results plotting) in the Andoyer-Deprit phase space is performed based on the numerical integration of the equations (2.21).

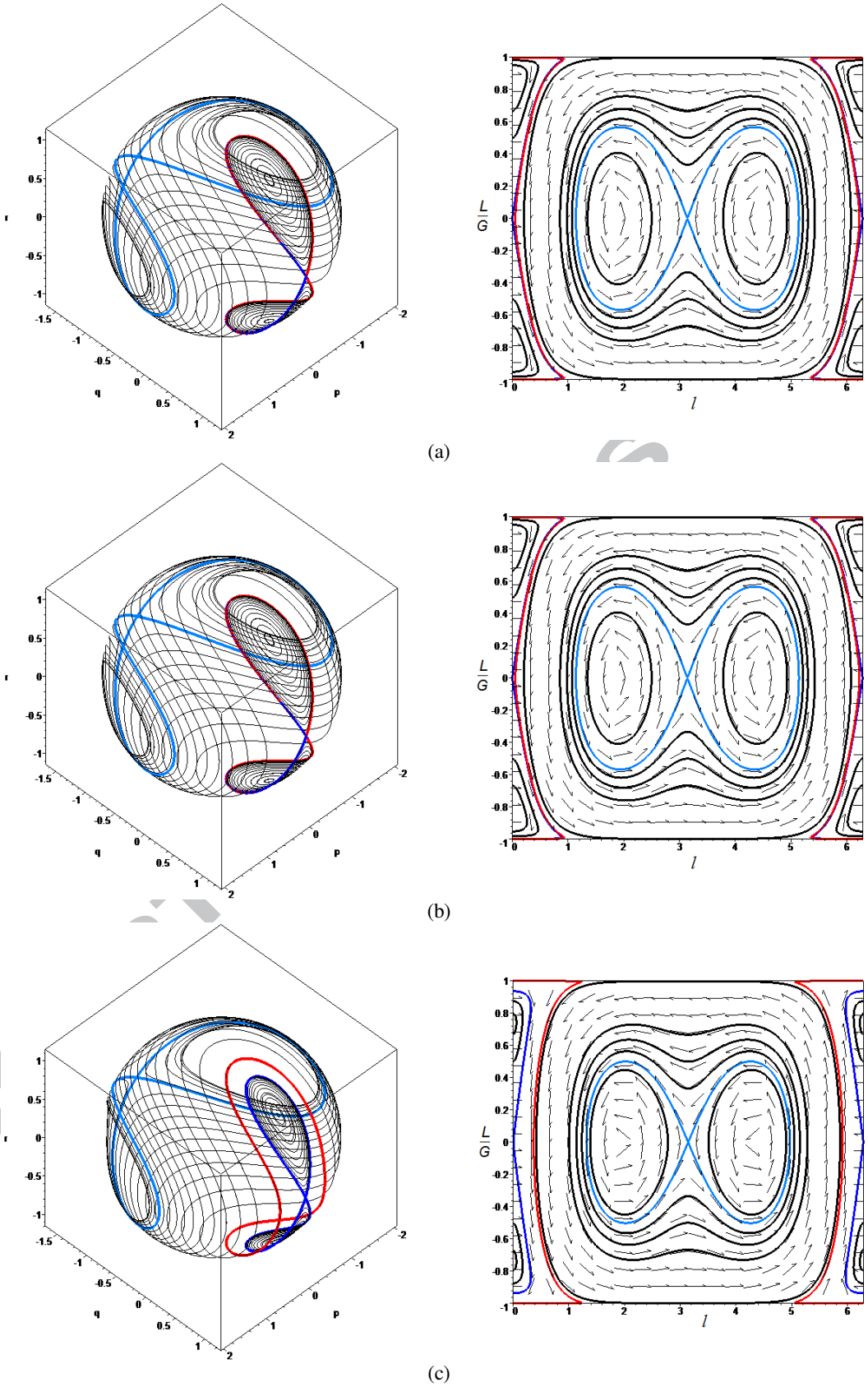

Fig.7 The correspondences between the angular momentum ellipsoid and the Andoyer-Deprit phase space
A=0.5, B=0.7, C=0.9 [kg·m^2]; K_*=1 [kg·m^2/s];
(a) D_{34}=0.10, (b) D_{34}=0.12, (c) D_{34}=0.15 [kg·m^2/s]

In this case we have the following values for constants (2.22) at the defined value q_*

$$2E = 2E_* = \hat{B}q_*^2 + 2T_R; \qquad K^2 = K_*^2 = \left(\hat{B}q_* + D_{34}\right)^2 \tag{2.37}$$

The coordinates of the saddle points are

$$\begin{aligned} &S_1\left(p=0;\ q=q_*;\ r=0\right);\\ &S_2\left(p=0;\ q=-\frac{K_*+D_{34}}{\hat{B}}=-q_*-\frac{2D_{34}}{\hat{B}};\ r=0\right) \end{aligned} \tag{2.38}$$

Similarly to the previous case we can write the dependences for the homoclinic polhode. Using expressions (2.15), (2.13), (2.37) ((2.13) with the multiplier $\hat{A}$) and the perfect square separating we can obtain the ellipse's dependence:

$$\begin{aligned} &\hat{C}\left(\hat{C}-\hat{A}\right)r^2 + \hat{B}\left(\sqrt{\hat{B}-\hat{A}}q + \frac{D_{34}}{\sqrt{\hat{B}-\hat{A}}}\right)^2 = P;\\ &P = K_*^2 - 2\hat{A}E_* + 2\hat{A}T_R - D_{34}^2 + \frac{\hat{B}D_{34}^2}{\hat{B}-\hat{A}} = \hat{B}\left[\sqrt{\hat{B}-\hat{A}}q_* + \frac{D_{34}}{\sqrt{\hat{B}-\hat{A}}}\right]^2 \end{aligned} \tag{2.39}$$

From (2.39) the expression follows

$$r = \pm\sqrt{\frac{\hat{B}}{\hat{C}\left(\hat{C}-\hat{A}\right)}}\sqrt{\left(\sqrt{\hat{B}-\hat{A}}q_* + \frac{D_{34}}{\sqrt{\hat{B}-\hat{A}}}\right)^2 - \left(\sqrt{\hat{B}-\hat{A}}q + \frac{D_{34}}{\sqrt{\hat{B}-\hat{A}}}\right)^2}$$

and in the rewritten form

$$r = \pm\sqrt{\frac{\hat{B}}{\hat{C}\left(\hat{C}-\hat{A}\right)}}\sqrt{\left(\left(\hat{B}-\hat{A}\right)\left[q_*+q\right] + 2D_{34}\right)\left[q_*-q\right]} \tag{2.40}$$

Using expressions (2.15), (2.13), (2.37) ((2.13) with the multiplier $\hat{C}$) and the perfect square separating we obtain once again the ellipse's dependence:

$$\begin{aligned} &\hat{A}\left(\hat{C}-\hat{A}\right)p^2 + \hat{B}\left[\sqrt{\left(\hat{C}-\hat{B}\right)}q - \frac{D_{34}}{\sqrt{\hat{C}-\hat{B}}}\right]^2 = R;\\ &R = \hat{C}\hat{B}q_*^2 - \left(\hat{B}q_* + D_{34}\right)^2 + D_{34}^2 + \frac{\hat{B}}{\hat{C}-\hat{B}}D_{34}^2 = \hat{B}\left(\sqrt{\left(\hat{C}-\hat{B}\right)}q_* - \frac{D_{34}}{\sqrt{\hat{C}-\hat{B}}}\right)^2 \end{aligned} \tag{2.41}$$

From (2.41) the expression follows

$$p = \pm\sqrt{\frac{\hat{B}}{\hat{A}\left(\hat{C}-\hat{A}\right)}}\sqrt{\left(\sqrt{\left(\hat{C}-\hat{B}\right)}q_* - \frac{D_{34}}{\sqrt{\hat{C}-\hat{B}}}\right)^2 - \left[\sqrt{\left(\hat{C}-\hat{B}\right)}q - \frac{D_{34}}{\sqrt{\hat{C}-\hat{B}}}\right]^2};$$

or in the rewritten form

$$p = \pm\sqrt{\frac{\hat{B}}{\hat{A}\left(\hat{C}-\hat{A}\right)}}\sqrt{\left(\left(\hat{C}-\hat{B}\right)[q_*+q]-2D_{34}\right)[q_*-q]}. \tag{2.42}$$

The coordinates of the loop-vertex points $V_{1,2}$ and $W_{1,2}$ are

$$\begin{aligned} q\left(V_{1,2}\right) &= q_V = -q_* + \frac{2D_{34}}{\left(\hat{C}-\hat{B}\right)}; \qquad p\left(V_{1,2}\right) = 0; \\ q\left(W_{1,2}\right) &= q_W = -q_* - \frac{2D_{34}}{\left(\hat{B}-\hat{A}\right)}; \qquad r\left(W_{1,2}\right) = 0. \end{aligned} \tag{2.43}$$

Now we can rewrite the second equation (2.17)

$$\dot{q} = \pm\frac{\sqrt{\left(\hat{B}-\hat{A}\right)\left(\hat{C}-\hat{B}\right)}}{\sqrt{\hat{A}\hat{C}}}\sqrt{[q_*+q]+\frac{2D_{34}}{\left(\hat{B}-\hat{A}\right)}}\sqrt{[q_*+q]-\frac{2D_{34}}{\left(\hat{C}-\hat{B}\right)}}[q_*-q]$$

and in the rewritten form

$$\dot{q} = \mp M\sqrt{[q_*-q]-a}\sqrt{[q_*-q]-b}\,[q_*-q]$$

$$a = 2q_* + \frac{2D_{34}}{\left(\hat{B}-\hat{A}\right)} > 0; \qquad b = 2q_* - \frac{2D_{34}}{\left(\hat{C}-\hat{B}\right)} > 0; \qquad M = \frac{\sqrt{\left(\hat{B}-\hat{A}\right)\left(\hat{C}-\hat{B}\right)}}{\sqrt{\hat{A}\hat{C}}}$$

The following quadrature takes place after the integration

$$\mp\int_0^t M dt = \int_{q_0}^{q}\frac{d[q-q_*]}{\sqrt{[q-q_*]+a}\sqrt{[q-q_*]+b}\,[q-q_*]} \tag{2.44}$$

It is the well-known standard integral [33]

$$\int\frac{dx}{x\sqrt{a_0+a_1x+a_2x^2}} = -\frac{1}{\sqrt{a_0}}\ln\frac{2a_0+a_1x+2\sqrt{a_0}\sqrt{a_0+a_1x+a_2x^2}}{x} \tag{2.45}$$

Using (2.45) the quadrature (2.44) can be rewritten

$$\begin{aligned} &\pm\int_0^t M dt = \int_{q_0}^{q}\frac{d[q_*-q]}{\sqrt{[q_*-q]-a}\sqrt{[q_*-q]-b}\,[q_*-q]} \\ &\int\frac{dx}{x\sqrt{a_0+a_1x+a_2x^2}} = -\frac{1}{\sqrt{a_0}}F(x); \\ &F(x) = \ln\frac{2a_0+a_1x+2\sqrt{a_0}\sqrt{a_0+a_1x+a_2x^2}}{x}; \\ &a_2 = 1;\ a_1 = a+b;\ \ a_0 = ab; \\ &\pm Mt = -\frac{1}{\sqrt{ab}}F(q-q_*)\Big|_{q_0}^{q} = -\frac{1}{\sqrt{ab}}\left[F(q-q_*)-F(q-q_*)\right]; \end{aligned} \tag{2.46}$$

Here we note the following circumstances:

1). At the solutions finding for the homoclinic loops with the saddle S_1 we have to take the coordinates of the vertices $V_{1,2}$ as the initial q-values:

$$q_0 = q_V = -b + q_*; \quad F(q_0 - q_*) = F(q_V - q_*) = \ln E_V; \quad E_V = b - a. \tag{2.47}$$

2). At the solutions finding for the homoclinic loops with the saddle S_2 we have to take the coordinates of the vertices $W_{1,2}$ as the initial q-values:

$$q_0 = q_W = -a + q_*; \quad F(q_0 - q_*) = F(q_W - q_*) = \ln E_W; \quad E_W = a - b. \tag{2.48}$$

So, the following solution takes place:

$$\pm\sqrt{ab}Mt = \ln \frac{2ab + (a+b)[q-q_*] + 2\sqrt{ab}\sqrt{([q-q_*]+a)([q-q_*]+b)}}{[q-q_*]\mathrm{Const}}; \tag{2.49}$$

where $\mathrm{Const} = \{E_V \text{ or } E_W\}$.

After some transformations the homoclinic dependence $q(t)$ follows from (2.49); and the reverse reductions give the homoclinic dependencies $p(t)$, $r(t)$:

$$q(t) = q_* + \frac{4ab\exp\left[\pm\sqrt{ab}Mt\right]\mathrm{Const}}{\left(\exp\left[\pm\sqrt{ab}Mt\right]\mathrm{Const} - a - b\right)^2 - 4ab}; \tag{2.50}$$
$$p(t) = p(q(t)); \qquad r(t) = r(q(t))$$

At the Fig.8 the full coincidence of the analytical results (2.50) with the numerical calculations is demonstrated.

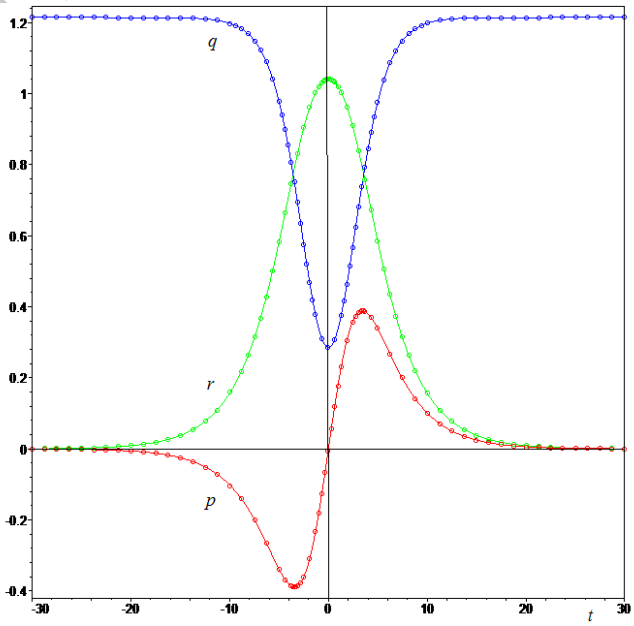

Fig.8 The homoclinic dependences:
the analytical results (points) and the numerical integrations (lines)
A=0.5, B=0.7, C=0.9 [kg·m^2]; K_*=1, D_{34}=0.15 [kg·m^2/s]

3.3. The general exact explicit solutions

Let's obtain the general form of exact solutions in the Jacobi elliptic functions. Similarly to the previous cases, using expressions (2.13), (2.15) ((2.13) with the multiplier $\hat{A}$) we can write the ellipse's dependence in the general form for the arbitrary values of the constants (2.22):

$$\begin{aligned} &\hat{C}\left(\hat{C}-\hat{A}\right)r^2+\hat{B}\left(\hat{B}-\hat{A}\right)\left(q+\frac{D_{34}}{\hat{B}-\hat{A}}\right)^2=P; \\ &P=K^2-2\hat{A}E\ +2\hat{A}T_R-D_{34}^2+\frac{\hat{B}D_{34}^2}{\hat{B}-\hat{A}}>0. \end{aligned} \tag{2.51}$$

Also with the help of (2.13) and (2.15) ((2.13) with the multiplier $\hat{C}$) we can write the following expression:

$$\begin{aligned} &\hat{A}\left(\hat{C}-\hat{A}\right)p^2+\hat{B}\left(\hat{C}-\hat{B}\right)\left[q-\frac{D_{34}}{\hat{C}-\hat{B}}\right]^2=R; \\ &R=2E\hat{C}-2T_R\hat{C}-K^2+D_{34}^2+\frac{\hat{B}}{\hat{C}-\hat{B}}D_{34}^2>0. \end{aligned} \tag{2.52}$$

With the help of (2.51) and (2.52) it is possible to express the *p*- and *r*-components of the angular velocity as the functions of the *q*-component, then the substitution of these expressions $\{p=p(q);\ r=r(q)\}$ into the second equation (2.17) gives us

$$\begin{aligned} &\frac{dq}{\sqrt{1-\gamma^2(q+\alpha)^2}\sqrt{1-\delta^2(q-\beta)^2}}=\pm\frac{\gamma\delta}{\hat{B}\sqrt{\hat{A}\hat{C}}}dt \\ &\alpha=D_{34}\Big/\left(\hat{B}-\hat{A}\right)>0; \qquad \beta=D_{34}\Big/\left(\hat{C}-\hat{B}\right)>0 \\ &\gamma^2=\hat{B}\left(\hat{B}-\hat{A}\right)\Big/P>0; \quad \delta^2=\hat{B}\left(\hat{C}-\hat{B}\right)\Big/R>0 \end{aligned} \tag{2.53}$$

Now we can use the change of the variables

$$z=\sqrt{\frac{(\alpha+1/\gamma+\beta-1/\delta)}{(\alpha+1/\gamma+\beta+1/\delta)}\frac{(q-\beta-1/\delta)}{(q-\beta+1/\delta)}} \tag{2.54}$$

Then after integration of (2.53) the quadrature follows

$$F(z,k)=\pm N\left[t-t_0\right]+I_0 \tag{2.55}$$

where the elliptic integral of the first kind $F(z,k)$ takes place [34]

$$\begin{aligned} &F(z,k)=\int_0^z\frac{dz}{\sqrt{1-z^2}\sqrt{1-k^2z^2}}; \quad k=\sqrt{\frac{(\alpha+\beta)^2-(1/\delta+1/\gamma)^2}{(\alpha+\beta)^2-(1/\delta-1/\gamma)^2}}<1; \\ &I_0=F(z_0,k)=\text{const}; \qquad N=\frac{\gamma^2\delta^2\sqrt{(\alpha+\beta)^2-(1/\delta-1/\gamma)^2}}{2\hat{B}\sqrt{\hat{A}\hat{C}}} \end{aligned}$$

After the inversion of the elliptic integral (2.55) we obtain the exact explicit solution in terms of elliptic functions ("amplitude" and "elliptic sine"):

$$z(t)=\mathrm{sn}\left(\pm N\left[t-t_0\right]+I_0,\ k\right) \tag{2.56}$$

where

$$\mathrm{sn}(u,k)=\sin\left(\varphi(u)\right),\quad \varphi(u)=\mathrm{am}(u,k)=\Phi^{-1}(u)$$
$$u=\Phi(\varphi)=\int_0^{\varphi}\frac{d\vartheta}{\sqrt{1-k^2\sin^2\vartheta}}=\pm N\left[t-t_0\right]+I_0$$

The reverse reductions give us the exact explicit solutions for the angular velocity's components $\{p,q,r\}$:

$$q(t)=\frac{(\alpha+1/\gamma+\beta+1/\delta)(\beta-1/\delta)\,\mathrm{sn}^2\left(\pm N\left[t-t_0\right]+I_0,\ k\right)-(\alpha+1/\gamma+\beta-1/\delta)(\beta+1/\delta)}{(\alpha+1/\gamma+\beta+1/\delta)\,\mathrm{sn}^2\left(\pm N\left[t-t_0\right]+I_0,\ k\right)-(\alpha+1/\gamma+\beta-1/\delta)};$$
$$p=p\left(q(t)\right);\qquad r=r\left(q(t)\right) \tag{2.57}$$

Also similarly to the articles [1-3, 28] if the vector of the angular momentum **K** is directed precisely along the axis *OZ* (it always can be realized by the *OXYZ*-frame rotation), we obtain the exact solutions for the Euler angles (ψ – the precession angle, θ – the nutation angle, φ – the intrinsic rotation angle):

$$\cos\theta(t)=\hat{C}r(t)\big/K;\quad \mathrm{tg}\,\varphi(t)=\frac{\hat{A}p(t)}{\hat{B}q(t)+D_{34}};$$
$$\psi(t)-\psi_0=\int_{t_0}^{t}K\frac{K_x p+K_y q}{K_x^2+K_y^2}dt=\int_{t_0}^{t}K\frac{\hat{A}p^2(t)+\left[\hat{B}q(t)+D_{34}\right]q(t)}{\hat{A}^2p^2(t)+\left[\hat{B}q(t)+D_{34}\right]^2}dt \tag{2.58}$$

In this case the following correspondences between Andoyer's-Deprit's and Euler's variables take place

$$\cos\theta=L/K;\ l=\varphi$$

The obtained solutions for the MSSC angular velocity (2.57) and for the Euler angles (2.58) are connected with results generalizing the classical tasks of the rigid body dynamics and corresponding applications, especially, with the angular motion of gyrostats, coaxial bodies and the dual-spin spacecraft – here we can indicate the important results [1-4, 22-29].

At the end of this section it is worth to underscore that as opposed to the previous MSSC-results [19] in this article the homoclinic and general solutions were found with the help of the polhodes' geometry analysis [2, 28, 31]. Also we additionally note that the MSSC homo/heteroclinic solutions in the article [19] were obtained by analogy with the DSSC solutions [30], which were found by V.S.Aslanov using the classical method of the differential equations integration [32] with the traditional analysis of the quantity/disposition/multiplicity of the polynomials roots at the elliptic (and in limits hyperbolic/trigonometric) quadratures evaluating – this approach is quite useful in the classical and modern tasks of rigid bodies dynamics [1-5, 24-27].

4. Chaos in the MSSC attitude dynamics

4.1. The perturbed system equations

Using the Hamiltonian (2.20) we can write the following equations for the positional part of the Andoyer-Deprit variables (for the subsystem $\{l, L\}$):

$$\begin{aligned}\dot{l} &= L\left[\frac{1}{\hat{C}}-\frac{\sin^2 l}{\hat{A}}-\frac{\cos^2 l}{\hat{B}}\right]+\frac{L}{\sqrt{G^2-L^2}}\left\{\frac{D_{12}\sin l}{\hat{A}}+\frac{D_{34}\cos l}{\hat{B}}\right\}-\frac{D_{56}}{\hat{C}}\\ \dot{L} &= \left(G^2-L^2\right)\left(\frac{1}{\hat{B}}-\frac{1}{\hat{A}}\right)\sin l\cos l+\sqrt{G^2-L^2}\left\{\frac{D_{12}\cos l}{\hat{A}}-\frac{D_{34}\sin l}{\hat{B}}\right\}\end{aligned} \tag{3.1}$$

Let us investigate the local chaos in the MSSC dynamics close to the homoclinic orbits under the influence of small harmonic perturbations in the internal engines of the rotors (1.9):

$$\dot{\Delta}_{ij} = -\varepsilon d_{ij}\sin\left(\nu_{ij}t+\psi_{ij}\right) \tag{3.2}$$

where $d_{ij}, \nu_{ij}, \psi_{ij}$ are the constants, corresponding to the *ij*-rotor (some of them can be equal to zero), and ε is the small parameter (ε<<1).

These harmonic perturbations are possible, for example, at the presence of harmonic errors in the signals of control/regulating/stabilizing systems – it can be due to the delays in the rate gyro units.

From (3.2) the solution directly follows

$$\Delta_{ij} = \Delta_{ij}(0)+\varepsilon\frac{d_{ij}}{\nu_{ij}}\left[\cos\left(\nu_{ij}t+\psi_{ij}\right)-\cos\psi_{ij}\right] \tag{3.3}$$

As it was realized in the previous sections, we take the same assumption (2.23). Then we have

$$\begin{aligned}&D_{12} = \sum_{j=1}^{N}\left[\Delta_{1j}(0)+\Delta_{2j}(0)\right]=0, \quad D_{56} = \sum_{j=1}^{N}\left[\Delta_{5j}(0)+\Delta_{6j}(0)\right]=0\\ &D_{34} = \sum_{j=1}^{N}\left[\Delta_{3j}(0)+\Delta_{4j}(0)\right]\neq 0\end{aligned} \tag{3.4}$$

Now it is possible to rewrite the canonical equations with the separation of the unperturbed ($f_{l,L}$) and ε-perturbed ($g_{l,L}$) parts

$$\dot{l} = f_l+\varepsilon g_l; \qquad \dot{L} = f_L+\varepsilon g_L \tag{3.5}$$

where

$$\begin{aligned}f_l &= L\left[\frac{1}{\hat{C}}-\frac{\sin^2 l}{\hat{A}}-\frac{\cos^2 l}{\hat{B}}\right]+\frac{D_{34}L\cos l}{\hat{B}\sqrt{G^2-L^2}};\\ f_L &= \left(G^2-L^2\right)\left(\frac{1}{\hat{B}}-\frac{1}{\hat{A}}\right)\sin l\cos l-\frac{D_{34}}{\hat{B}}\sqrt{G^2-L^2}\sin l;\\ g_l &= \frac{L}{\sqrt{G^2-L^2}}\left\{\frac{Q_{12}\sin l}{\hat{A}}+\frac{Q_{34}\cos l}{\hat{B}}\right\}-\frac{Q_{56}}{\hat{C}};\\ g_L &= \sqrt{G^2-L^2}\left\{\frac{Q_{12}\cos l}{\hat{A}}-\frac{Q_{34}\sin l}{\hat{B}}\right\};\end{aligned} \tag{3.6}$$

$$Q_{12}=\sum_{j=1}^{N}\left[\frac{d_{1j}}{\nu_{1j}}\left[\cos\left(\nu_{1j}t+\psi_{1j}\right)-\cos\psi_{1j}\right]+\frac{d_{2j}}{\nu_{2j}}\left[\cos\left(\nu_{2j}t+\psi_{2j}\right)-\cos\psi_{2j}\right]\right];$$
$$Q_{34}=\sum_{j=1}^{N}\left[\frac{d_{3j}}{\nu_{3j}}\left[\cos\left(\nu_{3j}t+\psi_{3j}\right)-\cos\psi_{3j}\right]+\frac{d_{4j}}{\nu_{4j}}\left[\cos\left(\nu_{4j}t+\psi_{4j}\right)-\cos\psi_{4j}\right]\right]; \quad (3.7)$$
$$Q_{56}=\sum_{j=1}^{N}\left[\frac{d_{5j}}{\nu_{5j}}\left[\cos\left(\nu_{5j}t+\psi_{5j}\right)-\cos\psi_{5j}\right]+\frac{d_{6j}}{\nu_{6j}}\left[\cos\left(\nu_{6j}t+\psi_{6j}\right)-\cos\psi_{6j}\right]\right].$$

4.2. The Melnikov function construction

In the case with polyharmonic perturbations the Melnikov function can be constructed as the "quasiperiodic Melnikov function" [36].

As indicated in [36] (Definition 4.1):

▼Function $f:\mathbb{R}\to\mathbb{R}$ is said to be quasiperiodic if there exists a C^r function $F:\mathbb{R}^l\to\mathbb{R}$ where F is 2π-periodic in each variable, i.e.,

$$F\left(\xi_1,...,\xi_i,...,\xi_l\right)=F\left(\xi_1,...,\xi_i+2\pi,...,\xi_l\right),\ \ \forall\xi\in\mathbb{R}^l,\ \ \forall i=1,...,l$$

and

$$f\left(t\right)=F\left(\omega_1 t,...,\omega_l t\right),\quad t\in\mathbb{R} \quad (3.8)$$

The real numbers $\omega_1,...,\omega_l$ are called the basic frequencies of $f(t)$. A vector-valued function is said to be quasiperiodic if each component is quasiperiodic in the above sense. ▲

So, in compliance with the above mentioned definition, we have the quasiperiodic vector-valued function Q with 6N basic frequencies ν_{ij} $\left(i=1..6,\ j=1..N\right)$:

$$Q\left(t\right)=F\left(\nu_{11}t,...,\nu_{6N}t\right)=\begin{bmatrix}Q_{12}\left(\nu_{1j}t,...,\nu_{2j}t\right)\\ Q_{34}\left(\nu_{3j}t,...,\nu_{4j}t\right)\\ Q_{56}\left(\nu_{5j}t,...,\nu_{6j}t\right)\end{bmatrix}. \quad (3.9)$$

Here we note that the values d_{ij}, ψ_{ij} in the functions Q_{ij} are the parameters connected only with the mechanical properties of the system (this set of parameters is essential for the system and can't vary during the mathematical transformations).

Then, following [36], for the one-degree-of-freedom Hamiltonian system with l-quasiperiodic perturbations we have the corresponding equations

$$\dot{x}=JDH\left(x\right)+\varepsilon g\left(x,\omega_1 t,...,\omega_l t;\mu,\varepsilon\right)$$
$$J=\begin{bmatrix}0 & 1\\ -1 & 0\end{bmatrix};\quad D=\left[\frac{\partial}{\partial x_1},\frac{\partial}{\partial x_2}\right]^T \quad (3.10)$$

This system also can be written in the autonomous form

$$\begin{cases} \dot{x} = JDH\left(x\right) + \varepsilon g\left(x, \theta_1, ..., \theta_l; \mu, \varepsilon\right) \\ \dot{\theta}_1 = \omega_1, \\ ... \\ \dot{\theta}_l = \omega_l, \end{cases} \tag{3.11}$$

where $\left(x, \theta_1, ..., \theta_l; \mu, \varepsilon\right) \in \mathbb{R}^2 \times T^l \times \mathbb{R}^p \times \mathbb{R}$, μ – is the parameters vector.

For the homoclinic orbit $x_h\left(t\right)$ of the unperturbed (ε=0) system (3.11) and for the Poincaré section by the angle θ_i (the repetition of the initial value $\theta_i\left(0\right) = \overline{\theta}_{i0}$: $\overline{\theta}_{i0} \to \overline{\theta}_{i0} + 2\pi$) the following quasiperiodic Melnikov function takes place [36]

$$M\left(t_0, \theta_{10}, ..., \overline{\theta}_{i0}, ..., \theta_{l0}; \mu\right) =$$
$$= \int_{-\infty}^{+\infty} \left\langle DH\left(x_h\left(t\right)\right), g\left(x_h\left(t\right), \omega_1\left(t + t_0\right) + \theta_{10}, ..., \omega_i\left(t + t_0\right) + \overline{\theta}_{i0}, ..., \omega_l\left(t + t_0\right) + \theta_{l0}; \mu, 0\right)\right\rangle dt \tag{3.12}$$

where $\left\langle \bullet, \bullet \right\rangle$ denotes the scalar product.

It is well-known fact, if at some point $\left(\tilde{t}_0, \tilde{\theta}_{10}, ..., \overline{\theta}_{l0}, ..., \tilde{\theta}_{l0}; \mu\right)$ the Melnikov function has the simple zero-root, then the intersection of stable and unstable manifolds of the homoclinic orbit takes place. Usually to the detection of the zero-roots of the Melnikov function only parameter t_0 may be used at the fixed "angle"-parameters $\left(\tilde{\theta}_{10}, ..., \overline{\theta}_{l0}, ..., \tilde{\theta}_{l0}\right)$ [36].

So, in our case we have the perturbed one-degree-of-freedom Hamiltonian system (3.5) with the quasiperiodic perturbation, where $x = \left(l, L\right)$ - is the main coordinates and $\theta_{ij} = \nu_{ij} t$ - are the angle-variables. Using the expressions (2.9)-(2.11) and (3.4) it is possible to rewrite the functions (3.6) in the following form

$$f_l\left(l, L\right) = f_l\left(p, q, r\right) = \hat{C} r \left[\frac{1}{\hat{C}} - \frac{\hat{B}\hat{A}p^2 + \left(\hat{B}q + D_{34}\right)^2 + D_{34}\left(\hat{B}q + D_{34}\right)}{\hat{B}\left(G^2 - \hat{C}^2 r^2\right)}\right];$$
$$f_L\left(l, L\right) = f_L\left(p, q, r\right) = \left(\frac{1}{\hat{B}} - \frac{1}{\hat{A}}\right)\hat{A}p\left(\hat{B}q + D_{34}\right);$$
$$g_l\left(l, L, \theta_{ij}\right) = g_l\left(p, q, r, \theta_{ij}\right) = \tag{3.13}$$
$$= \frac{\hat{C} r}{\left(G^2 - \hat{C}^2 r^2\right)}\left\{\frac{Q_{12}\left(\theta_{1j}, ..., \theta_{2j}\right)\hat{A}p}{\hat{A}} + \frac{Q_{34}\left(\theta_{3j}, ..., \theta_{4j}\right)\left(\hat{B}q + D_{34}\right)}{\hat{B}}\right\} - \frac{Q_{56}\left(\theta_{5j}, ..., \theta_{6j}\right)}{\hat{C}};$$
$$g_L\left(l, L, \theta_{ij}\right) = g_L\left(p, q, r, \theta_{ij}\right) = \left\{\frac{Q_{12}\left(\theta_{1j}, ..., \theta_{2j}\right)\left(\hat{B}q + D_{34}\right)}{\hat{A}} - \frac{Q_{34}\left(\theta_{3j}, ..., \theta_{4j}\right)\hat{A}p}{\hat{B}}\right\}.$$

The mechanical characteristics of the rotors' real angular motion are connected with the parameters d_{ij}, ψ_{ij}, therefore in the framework of the mathematical part of the task we can assign zero starting conditions for the associated angle-variables θ_{ij} $\left(\theta_{ij}\left(0\right) = 0, \ \forall i, j\right)$. Also we can

define the Poincaré map as the section by the θ_{31}- angle (certainly, we could take any other angle-variable):

$$P^{\theta_{310}}:\ \bar{\theta}_{310} \to \bar{\theta}_{310} + 2\pi$$

With the help of expressions (3.13) the quasiperiodic Melnikov function is written in the form

$$M\left(t_0, \theta_{110}, ..., \bar{\theta}_{310}, ..., \theta_{6N0}\right) =$$
$$= \int_{-\infty}^{+\infty} \left[f_L\left(p(t), q(t), r(t)\right) g_l\left(p(t), q(t), r(t), \theta_{ij}(t+t_0)\right) - \right. \tag{3.14}$$
$$\left. - f_l\left(p(t), q(t), r(t)\right) g_L\left(p(t), q(t), r(t), \theta_{ij}(t+t_0)\right) \right] dt,$$

where $\theta_{ij}(t+t_0) = \nu_{ij}(t+t_0) + \theta_{ij0}$ $(\forall i, j)$; the homoclinic dependences $\{p(t), q(t), r(t)\}$ correspond to the exact homoclinic solutions (2.50) and/or (2.36).

In this paper we focus only at the numerical analysis and simulations of the system's chaotic behavior. The analytical investigation of the Melnikov function (3.14) and the antichaotization conditions obtaining are the prospective tasks for independent research. So, in the next section we will present the main simulations of the perturbed system behavior, including the case of the system regular response under the influence of the polyharmonic disturbances.

4.3. Numerical simulations of the system chaotic regimes

4.3.1. The system chaotic motion under the influence of the single-harmonic perturbation

First of all, we can simulate the system motion with only one disturbance corresponding to the small single-harmonic perturbation at the rotor #31:

$$Q_{34} = \frac{d_{31}}{\nu_{31}} \left[\cos\left(\nu_{31} t + \psi_{31}\right) - \cos\psi_{31} \right] \tag{3.15}$$

In this case the numerical investigation gives us the following results: the time dependence (the time-history) (fig.9-a), the perturbed S_1-homoclinic trajectory (fig.9-b), the Poincaré section of the S_1-homoclinic trajectory in the space of the angular velocity components (fig.9-c), the Poincaré section of the S_2-homoclinic trajectory in the space of the angular velocity components (fig.9-d), the Poincaré section of the system's phase flow in the space of the angular velocity components (fig.9-e), the Poincaré section of the system's phase flow in the Andoyer-Deprit space (fig.9-f).

As we can see, the chaotic features of the MSSC motion appear ex facte. It also could be confirmed with the help of the Melnikov function evaluation (fig.10-a). We should note that at the Melnikov function evaluation (fig.10-a) only t_0 parameter was varied [36] with all fixed $\theta_{ij0} = 0$. The Melnikov function has the harmonic form with the infinite set of the simple roots, and, therefore, the intersections of stable and unstable manifolds of the homoclinic trajectory take place – this effect generate so-called homoclinic nets. The homoclinic nets (fig.10-b, c, d) were plotted as the sets of the Poincaré-map-images of the unperturbed homoclinic trajectory [31]: we separately plot the forward (in the forward direction of the time $t: 0 \to +\infty$) Poincaré-map-iterations and the backward (in the back direction of the time $t: 0 \to -\infty$) Poincaré-map-iterations.

The numerical simulations (fig.9, 10) were performed at the following parameters:

$$\hat{A} = 0.5,\ \ \hat{B} = 0.7,\ \ \hat{C} = 0.9\ [kg \cdot m^2];\ D_{34} = 0.5,\ K = 2.45\ [kg \cdot m^2 / s];$$
$$d_{31} = 1\ [kg \cdot m^2 / s^2];\ \nu_{31} = 2\ [1/s];\ \psi_{31} = 0;\quad \varepsilon = 0.06.$$

4.3.2. The system chaotic motion under the influence of the three-harmonic perturbation

Now we present the simulation of the system motion under the influence of the small perturbations at the rotors ## 11, 31, 51:

$$\begin{cases} Q_{12} = \dfrac{d_{11}}{\nu_{11}}\left[\cos\left(\nu_{11}t+\psi_{11}\right)-\cos\psi_{11}\right] \\ Q_{34} = \dfrac{d_{31}}{\nu_{31}}\left[\cos\left(\nu_{31}t+\psi_{31}\right)-\cos\psi_{31}\right] \\ Q_{56} = \dfrac{d_{51}}{\nu_{51}}\left[\cos\left(\nu_{51}t+\psi_{51}\right)-\cos\psi_{51}\right] \end{cases} \tag{3.16}$$

with the following parameters:

$$\hat{A}=0.5,\ \ \hat{B}=0.7,\ \ \hat{C}=0.9\ [kg\cdot m^2];\ \ D_{34}=0.5,\ \ K=3.16\ [kg\cdot m^2/s];\ \ \varepsilon=0.01;$$

$$d_{11}=1\ [kg\cdot m^2/s^2];\ \ \nu_{11}=3.5\ [1/s];\ \ \psi_{31}=1;$$

$$d_{31}=1\ [kg\cdot m^2/s^2];\ \ \nu_{31}=2.5\ [1/s];\ \ \psi_{31}=0;$$

$$d_{51}=1\ [kg\cdot m^2/s^2];\ \ \nu_{51}=1.5\ [1/s];\ \ \psi_{51}=2.$$

As the result we see the typical chaotic features of the motion (fig.11): the phase portraits have the well-defined chaotic layers; the Melnikov function has the polyharmonic form with the simple roots; the homoclinic net is very complicated.

4.3.3. The system regular motion under the influence of the three-harmonic perturbation

In this section we present the results (fig.12) of the system motion modeling with the same disturbances (3.16), but at the different values of the parameters:

$$\hat{A}=0.5,\ \ \hat{B}=0.7,\ \ \hat{C}=0.9\ [kg\cdot m^2];\ \ D_{34}=0.5,\ \ K=2.45\ [kg\cdot m^2/s];\ \ \varepsilon=0.02;$$

$$d_{11}=1\ [kg\cdot m^2/s^2];\ \ \nu_{11}=8\ [1/s];\ \ \psi_{31}=1;$$

$$d_{31}=1\ [kg\cdot m^2/s^2];\ \ \nu_{31}=10\ [1/s];\ \ \psi_{31}=0;$$

$$d_{51}=1\ [kg\cdot m^2/s^2];\ \ \nu_{51}=6\ [1/s];\ \ \psi_{51}=2.$$

As the result we obtain the regular dynamical process (fig.12): the time-history of the angular velocity components is periodic (fig.12-a); the perturbed homoclinic polhode is the regular twisted closed curve (fig.12-b); the Melnikov function is negative and has not any roots (fig.12-c); the Poincaré sections include only regular invariant curves without any chaotic regions (fig.12-d,f). Also we'd like to emphasize the simple spectrum (with separated frequencies) of the Fourier transform for the $p(t)$-signal (fig.12-e). All of the listed features are the typical attributes of the regular dynamical process.

The mentioned aspects of the regularization of the local homoclinic dynamics under the influence of the polyharmonic perturbations are connected, probably, with the following phenomena [42-45]:

- Regular synchronization of complicated nonlinear quasiperiodic oscillations (autooscillations) in dynamical systems with corresponding bifurcations and phase portraits' reconfigurations;
- Chaos synchronization as a phenomenon of periodic regimes' occurrences in chaotic oscillations (autooscillations) under external influences (periodic/chaotic/stochastic); and also coupled (drive-respond) chaotic systems synchronizations;
- Resonance initiation phenomenon (resonance tuning) in chaotic motions.

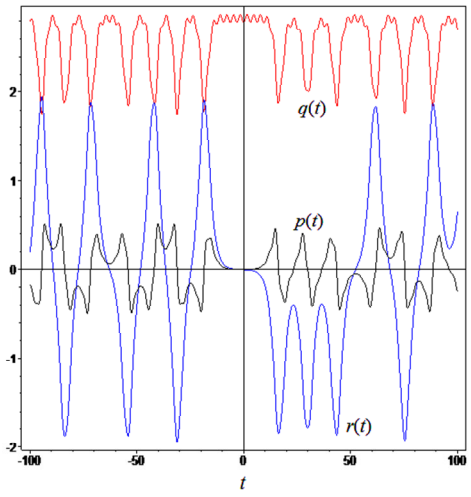

(a)

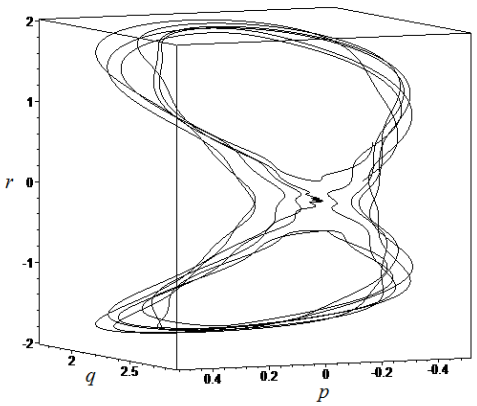

(b)

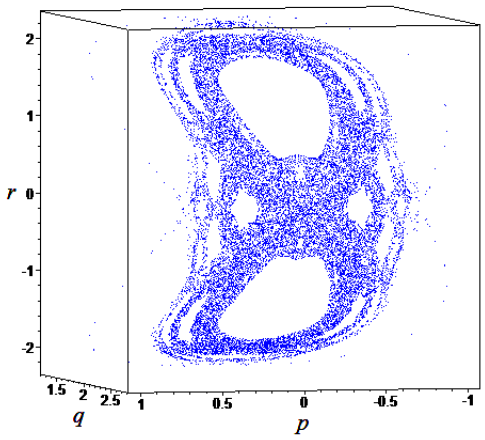

(c)

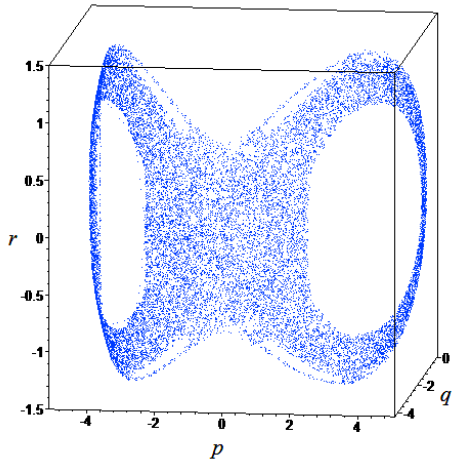

(d)

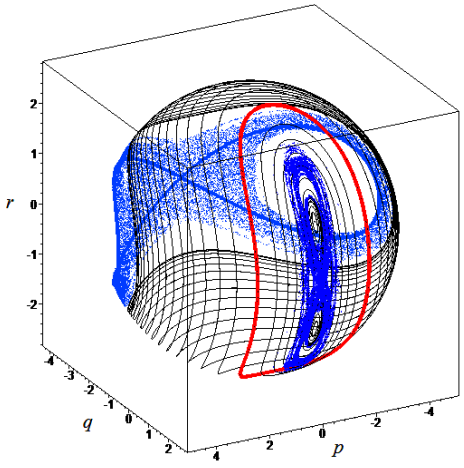

(e)

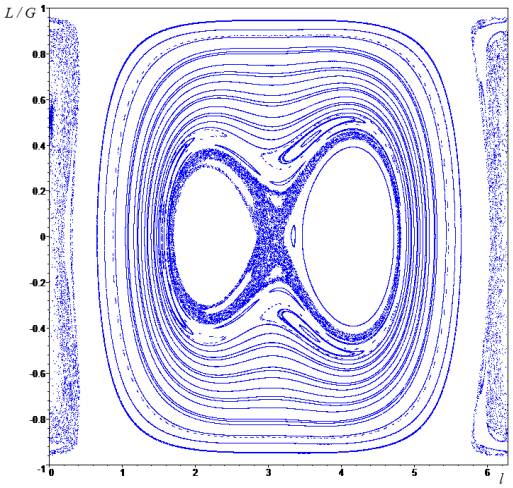

(f)

Fig.9 The results of the numerical simulations

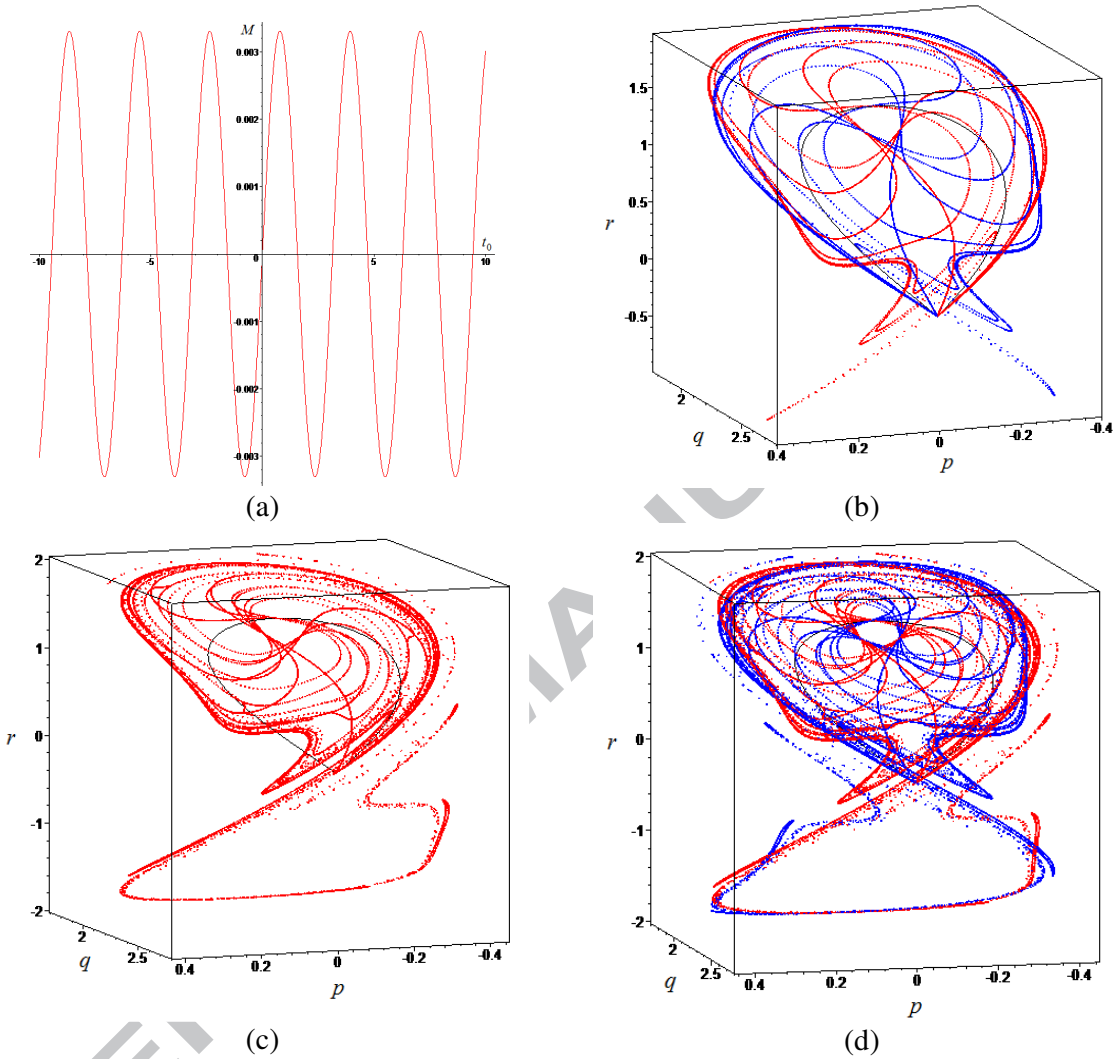

Fig.10 The Melnikov function (a) and the homoclinic nets:
(a) – the Melnikov function; (b) – five forward (red) and back (blue) Poincaré-map-images of the homoclinic separatrix;
(c) – ten forward Poincaré-map-images of the homoclinic separatrix; (d) – ten forward (red) and
back (blue) Poincaré-map-images of the homoclinic separatrix

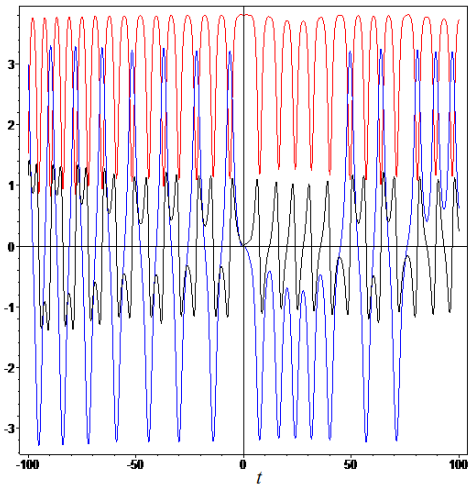

(a)

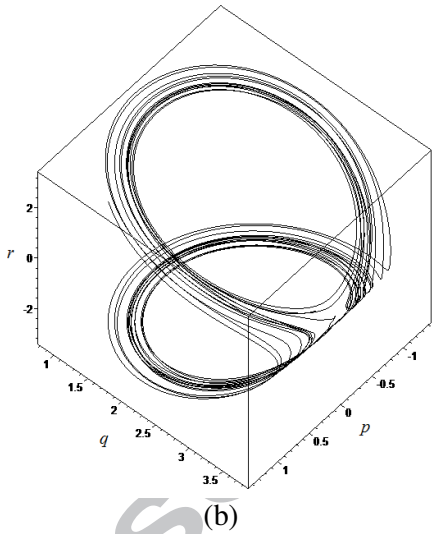

(b)

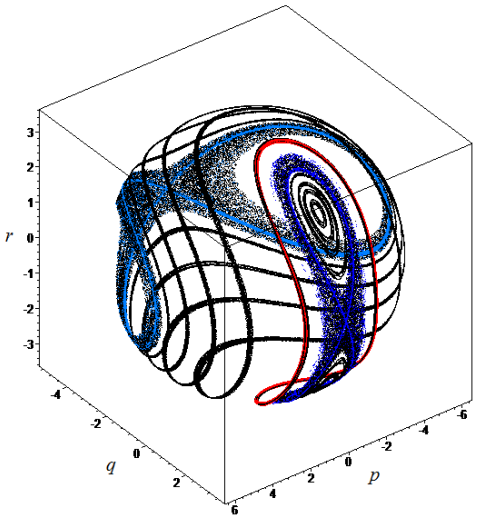

(c)

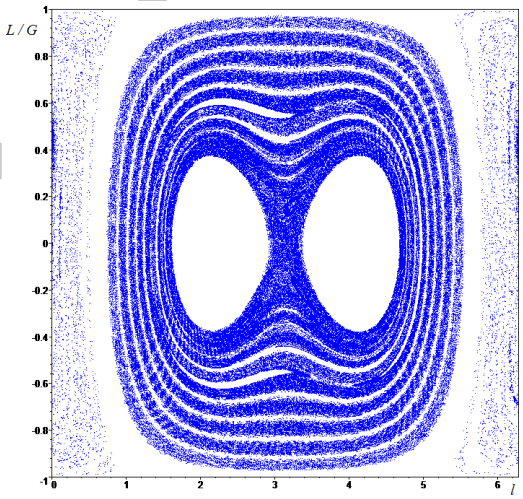

(d)

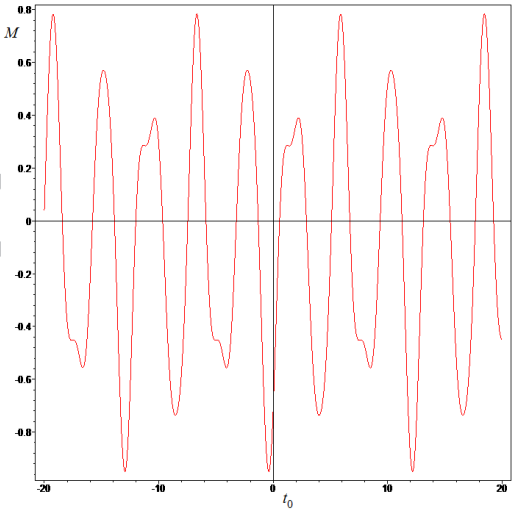

(e)

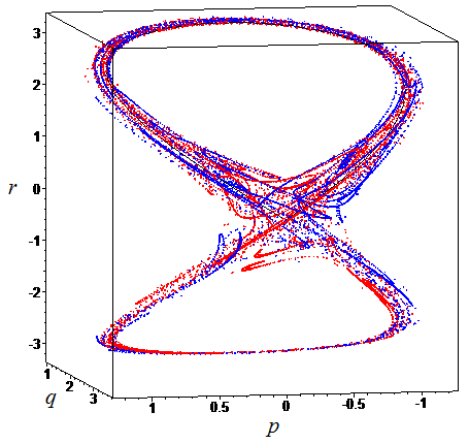

(f)

Fig.11 The results of the numerical simulation (the chaotic motion):
(a) – the time-history of the angular velocity components (p(t)-black, q(t)-red, r(t)-blue); (b) – the perturbed homoclinic trajectory; (c) – the Poincaré-map in the space of the angular velocity components; (d) - the Poincaré-map in the Andoyer-Deprit space; (e) – the Melnikov function; (f) – the homoclinic net as ten forward and back images of the homoclinic separatrix

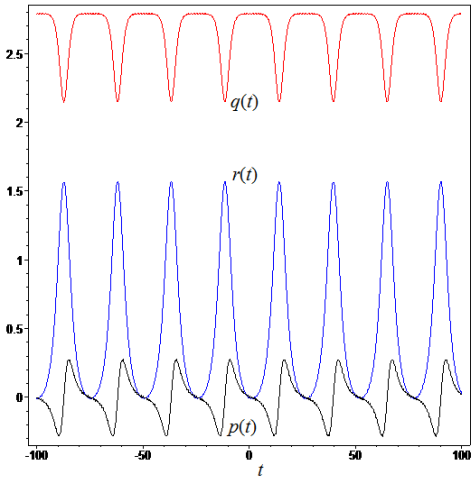

(a)

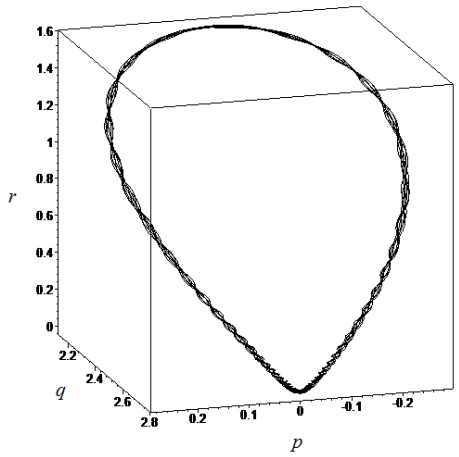

(b)

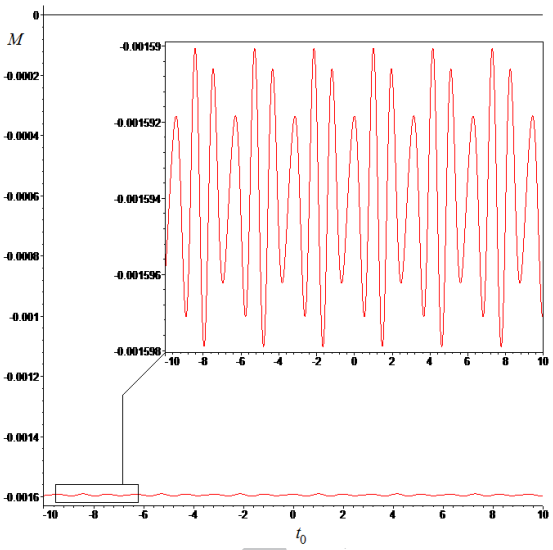

(c)

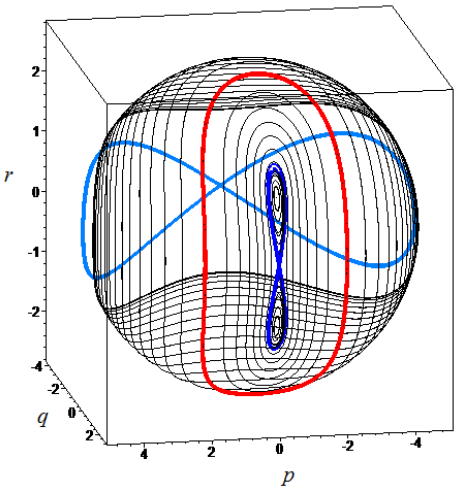

(d)

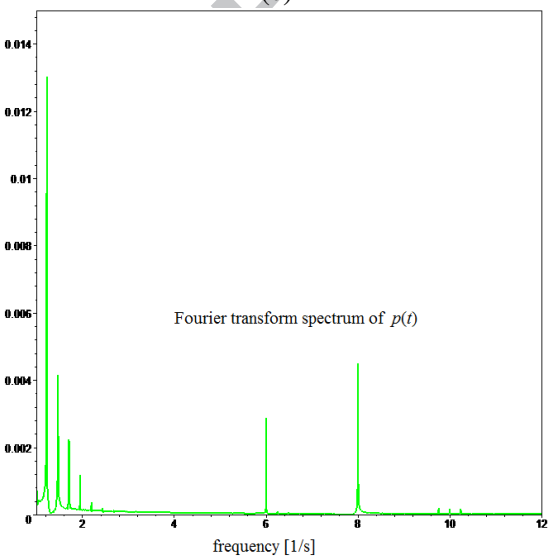

(e)

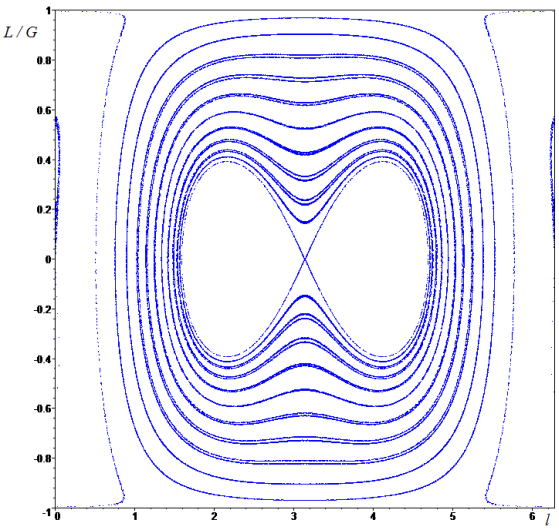

(f)

Fig.12 The results of the numerical simulation (the regular motion)

The advanced study of the listed phenomena in the MSSC's dynamics is the important independent research task, which can be considered in further separate publications. Here we have to repeat the statement that the Melnikov function is one of the main mathematical instruments for the local homoclinic chaotization/regularization investigation: the analytical structure of this function allows to obtain explicit conditions of the realization of local chaotic/regular modes.

Also the harmonic analysis and the Fourier transformation are the very useful tool: it is well-known that the chaotic modes have broad "continuous" spectrums, and, on the contrary, the regular regimes have simple discrete spectrums (with discrete frequencies). For the illustration of the last assertion we present (fig.13) the Fourier transform spectrum of the "$p(t)$-signal" for the considered cases 4.3.1-4.3.3.

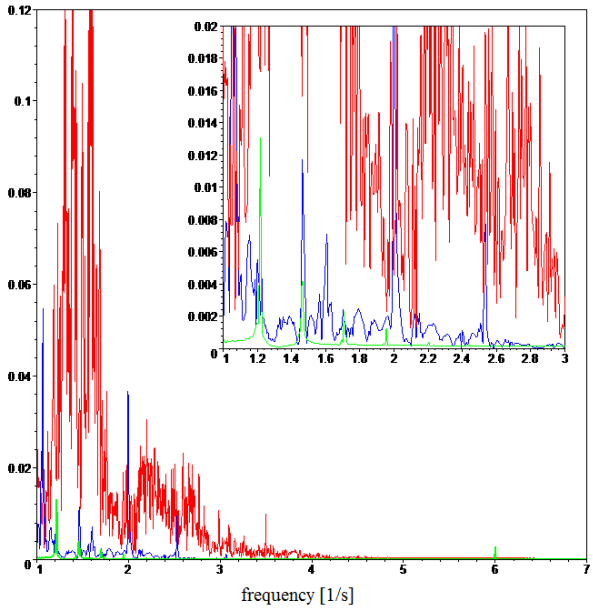

Fig. 13 The Fourier transform spectrum of the $p(t)$-component:
blue – the chaotic case (4.3.1); red – the chaotic case (4.3.2); green – the regular case (4.3.3)

5. Additional applications

In this section the possible applications of the multi-rotor system are shortly described. Also some future-technology vehicles are offered.

5.1. Gyroscopic stabilization, gyrostats and gyrostat-satellites

In the previous sections we considered the attitude dynamics of the multi-spin spacecraft. The main features of the MSSC motion are connected with the multi-rotor system (the multi-rotor kernel). This kernel allows to perform the attitude gyroscopic stabilization by the rotors' spinup. This method is usually applied to the dual-spin spacecraft and gyrostat-satellites attitude stabilization. So, we can use the multi-rotor MSSC in the DSSC-mode and also in the gyrostat-mode.

We'd like to note that the considered multi-rotor system has various independent internal degrees of freedom corresponding to the rotors' rotations. It is the powerful instrument for the support of the spacecraft's attitude stabilization with the help of the internal redistribution of the gyrostatic angular momentum between the rotors and the main body.

Also this multi-rotor system can be used for the investigation of the non-regular motion (with strange attractors) of gyrostats in resistant environments and gyrostat-satellites with complex feedbacks [41].

5.2. The attitude reorientation of the spacecraft

The considered in this paper multi-rotor systems allow fulfill series of the rotors' spinups and captures to perform the angular reorientation of the SC [18]. For the realization of the reorientation maneuver we have to perform the conjugated spinup (in the opposite directions) of the pair of conjugated rotors, and then stop one of them. After this capture the rotor's angular momentum is transmitted to the main rigid body of the SC, which performs the rotation around the corresponding axis. The capture of the second conjugated rotor compensates the angular momentum and stops the rotation of the SC's main body.

This approach of the attitude reorientation is characterized by the minimal motion inertia (or, moreover, by the inertia absence): it means the immediate redistribution of the angular momentum between the rotors and the SC's main body. It is possible if we fulfill the immediate rotors' captures with the help of the large friction generation or the gear meshing (or other types of slip-free engagements). This inertialess feature of the SC's angular motion is unique as compared with the classical attitude control realization by the reaction-wheels: as it was presented in [18], we can synthesize the piecewise constant angular velocity of the SC's main body without any noticeable transient regimes. Also it is possible to perform the compound spatial reorientation (the spatial rotation series) with the help of the corresponding conjugated spinup-capture-series for the rotors placed in several independent layers (fig.1-b).

The inertialess reorientation method is applicable for many types of the SC because the multi-rotor kernels can be constructed as quite small devices, which can be placed even in the nanosatellites.

5.3. Roll-walking multi-rotor robots and vehicles

One of the interesting applications of the considered multi-rotor system is roll-walking (somersaulting) multi-rotor robots and vehicles [20, 21].

So, it is possible to use the internal multi-rotor system as the drive kernel of the roll-walking robots and vehicles (fig.14). The multi-rotor drive kernel allows to perform the roll-walking somersaulting motion: to make one step we should turn over the robot body with the help of the conjugated spinup-capture.

For the realization of the roll-walking somersaulting step (the “somersault” around the edge) with the one-axis conjugated spinup/capture we can use two ground-fixed points ($\boldsymbol{G}_1$ and $\boldsymbol{G}_2$). And only one ground-fixed point ($\boldsymbol{G}_1$) is needed to turn over the robot’s body at the double-axis conjugated twofold spinup/capture with the gyroscopic torque initiation.

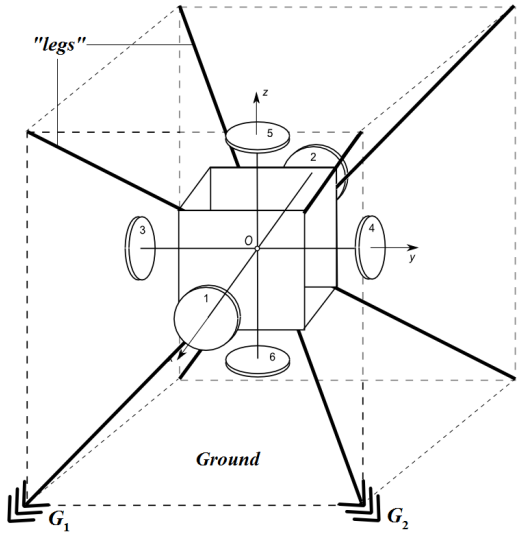

Fig. 14 The possible form of the roll-walking robot

5.4. Suppressions of the SC chaotic regimes with the help of the internal multi-rotor kernels

As it was described in the previous section (4.3.3) the regularization of the local chaotic motion takes place under the influence of the special defined polyharmonic torques in the rotors' engines. This feature we can use for the initiation of corresponding small polyharmonic torques in the rotors' engines to avoid the chaotic regimes. This important «antichaotization» task with constructing of «the internal antichaotization multi-rotor kernel» of the spacecraft can be considered in the independent separate research.

In this framework we can use many dynamical tools such as control techniques with the feedbacks, the resonance tuning, the initiation of dominating oscillations with suppressions of the «chaotic» frequencies.

5.5. The approach to modeling of the angular motion dynamics of an elastic body at small elastic vibrations

The mechanical and mathematical multi-rotors models developed in the previous sections can be applied to the modeling of the angular motion of an elastic body. We can consider the layers of the rotors as rotationally oscillating masses attached to the rigid body (the core body) by elastic connections (angular springs). Choosing the angular spring's stiffnesses c_{ij} (corresponding to the vibration eigenfrequencies of the elastic body) and the mass-inertia parameters of the rotors' (corresponding to the eigenmodes) we can consider the angular motion of the elastic body with the help of the simple dynamical system in the Hamiltonian form:

$$\begin{cases} H = \mathrm{T} + \Pi, \qquad x = \{l, \varphi_2, \varphi_3, \delta_{ij}\}, \qquad X = \{L, G, H, \Delta_{ij}\} \\ \mathrm{T} = \dfrac{G^2 - L^2}{2}\left[\dfrac{\sin^2 l}{\hat{A}} + \dfrac{\cos^2 l}{\hat{B}}\right] + \dfrac{1}{2\hat{C}}\left(L - D_{56}\right)^2 - \sqrt{G^2 - L^2}\left\{\dfrac{D_{12}\sin l}{\hat{A}} + \dfrac{D_{34}\cos l}{\hat{B}}\right\} + \dfrac{D_{12}^2}{2\hat{A}} + \dfrac{D_{34}^2}{2\hat{B}} + T_R \\ D_{12} = \sum_{j=1}^{N}\left[\Delta_{1j} + \Delta_{2j}\right]; \quad D_{34} = \sum_{j=1}^{N}\left[\Delta_{3j} + \Delta_{4j}\right]; \quad D_{56} = \sum_{j=1}^{N}\left[\Delta_{5j} + \Delta_{6j}\right]; \qquad T_R = \dfrac{1}{2}\sum_{j=1}^{N}\sum_{i=1}^{6}\dfrac{\Delta_{ji}^2}{I_j} \\ \Pi = \Pi\left(\delta_{ij}\right) = \dfrac{1}{2}\sum_i\sum_j c_{ij}\delta_{ij}^2; \qquad R = R\left(\sigma_{ij}\right) = \dfrac{1}{2}\sum_i\sum_j b_{ij}\sigma_{ij}^2 \end{cases}$$

Certainly, the selection of the springs' stiffness and the rotors' mass-inertia parameters should be carried out with the help of the special methods of the definition of the distributed oscillations' parameters of elastic bodies, or experimentally. For the additional modeling of the dissipation properties of the elastic body the standard Rayleigh's dissipation function $R\left(\sigma_{ij}\right)$ is quite useful.

Conclusion

So, in this paper the MSSC attitude dynamics was considered, the homoclinic and general exact solutions were obtained, the cases of the chaotic and regular motion under the influence of the polyharmonic disturbances were investigated.

ACKNOWLEDGMENTS

This work was supported by the Russian Foundation for Basic Research (RFBR ## 11-08-00794-a, 12-08-09202-mob-z).

REFERENCES

1. V.V. Golubev, Lectures on Integration of the Equations of Motion of a Rigid Body about a Fixed Point. Moscow: State Publishing House of Theoretical Literature, 1953.
2. J. Wittenburg, Dynamics of Systems of Rigid Bodies. Stuttgart: Teubner, 1977.
3. J. Wittenburg, Beitrage zur dynamik von gyrostaten, Accademia Nazional dei Lincei, Quaderno N. 227 (1975).
4. U.A. Arkhangelski, Analytical rigid body dynamics. Moscow: Nauka, 1977.
5. E. Leimanis, The general problem of the motion of coupled rigid bodies about a fixed point. Berlin: Springer-Verlag, 1965.
6. H. Andoyer, Cours de Mecanique Celeste, Paris: Gauthier-Villars, 1923.
7. A. Deprit, A free rotation of a rigid body studied in the phase plane, American Journal of Physics 35 (1967) 424 – 428.
8. P. W. Likins, Spacecraft Attitude Dynamics and Control - A Personal Perspective on Early Developments, J. Guidance Control Dyn. Vol. 9, No. 2 (1986) 129-134.
9. D. L. Mingori, Effects of Energy Dissipation on the Attitude Stability of Dual-Spin Satellites, AIAA Journal, Vol. 7, No. 1 (1969) 20-27.
10. P. M. Bainum, P. G. Fuechsel, D. L. Mackison, Motion and Stability of a Dual-Spin Satellite With Nutation Damping, Journal of Spacecraft and Rockets, Vol. 7, No. 6 (1970) 690-696.
11. K. J. Kinsey, D. L. Mingori, R. H. Rand, Non-linear control of dual-spin spacecraft during despin through precession phase lock, J. Guidance Control Dyn. 19 (1996) 60-67.
12. C. D. Hall, Momentum Transfer Dynamics of a Gyrostat with a Discrete Damper, J. Guidance Control Dyn., Vol. 20, No. 6 (1997) 1072-1075.
13. C.D. Hall, R.H. Rand, Spinup Dynamics of Axial Dual-Spin Spacecraft. Journal of Guidance, Control, and Dynamics, Vol. 17, No. 1 (1994) 30–37.
14. E.A. Ivin, Decomposition of variables in task about gyrostat motion, Mathematics and Mechanics series, no.3, Vestnik MGU (Transactions of Moscow's University), 1985, Pp.69–72.
15. Awad El-Gohary, New control laws for stabilization of a rigid body motion using rotors system, Mechanics Research Communications, Volume 33, Issue 6 (2006) 818-829.
16. A.V. Doroshin, Synthesis of Attitude Motion of Variable Mass Coaxial Bodies. WSEAS Transactions on Systems and Control, Issue 1, Volume 3 (2008) 50-61.
17. A.V. Doroshin, Analysis of attitude motion evolutions of variable mass gyrostats and coaxial rigid bodies system, International Journal of Non-Linear Mechanics, Volume 45, Issue 2 (2010) 193–205.
18. A.V. Doroshin, Attitude Control of Spider-type Multiple-rotor Rigid Bodies Systems. Proceedings of the World Congress on Engineering 2009, London, U.K. Vol II, pp.1544-1549.
19. A.V. Doroshin, Hamiltonian Dynamics of Spider-Type Multirotor Rigid Bodies Systems. Current Themes in Engineering Science 2009. AIP. Melville, New York, 2010. V.1220. Pp.27-42 (AIP Conference Proceedings 1220 , pp. 27-42).
20. A.V. Doroshin, Plenary Lecture 4: Attitude Dynamics and Control of Multi-Rotor Spacecraft and Roll-Walking Robots. Recent research in Communications, Electronics, Signal Processing & Automatic Control. – Proceedings of the 11th WSEAS International Conference on Signal Processing, Robotics and Automation (ISPRA'12). Cambridge, UK, 2012. P.15.
21. A.V. Doroshin, Motion Dynamics of Walking Robots with Multi-Rotor Drive Systems. Recent research in Communications, Electronics, Signal Processing & Automatic Control. – Proceedings of the 11th WSEAS International Conference on Signal Processing, Robotics and Automation (ISPRA'12). Cambridge, UK, 2012. Pp.122-126.
22. V. Volterra, Sur la théorie des variations des latitudes. Acta Math. 22 (1899).
23. N.E. Zhykovski, On the motion of a rigid body with cavities filled with a homogeneous liquid. Collected works, 1, Moscow-Leningrad, Gostekhisdat, 1949.
24. A. Elipe, V. Lanchares, Exact solution of a triaxial gyrostat with one rotor, Celestial Mechanics and Dynamical Astronomy, Issue 1-2, Volume 101, 2008, pp 49-68.
25. I. Basak, Explicit solution of the Zhukovski-Volterra gyrostat, Regular and chaotic dynamics Vol.14, N.2 (2009) 223-236.
26. V.S. Aslanov, Behavior of Axial Dual-spin Spacecraft, Proceedings of the World Congress on Engineering 2011, WCE 2011, 6-8 July, 2011, London, U.K., pp. 13-18.
27. V.S. Aslanov, Integrable cases in the dynamics of axial gyrostats and adiabatic invariants, Nonlinear Dynamics, Volume 68, Numbers 1-2 (2012) 259-273.
28. A.V. Doroshin, Exact solutions for angular motion of coaxial bodies and attitude dynamics of gyrostat-satellites. International Journal of Non-Linear Mechanics, Volume 50 (2013) 68-74.
29. Jinlu Kuang, Soonhie Tan, Kandiah Arichandran, A.Y.T. Leung, Chaotic dynamics of an asymmetrical gyrostat, International Journal of Non-Linear Mechanics, Volume 36, Issue 8 (2001) 1213-1233.
30. V.S. Aslanov, A.V. Doroshin, Chaotic dynamics of an unbalanced gyrostat. Journal of Applied Mathematics and Mechanics, Volume 74, Issue 5 (2010) 525-535.

31. A.V. Doroshin, Heteroclinic dynamics and attitude motion chaotization of coaxial bodies and dual-spin spacecraft, Communications in Nonlinear Science and Numerical Simulation, Volume 17, Issue 3 (2012) 1460–1474.
32. M. Tabor, Chaos and Integrability in Nonlinear Dynamics: An Introduction. Wiley, John & Sons, New York, 1989.
33. Gradshteyn I.S., Ryzhik I.M. Table of integrals, series and products. San Diego: Academic Press; 1980.
34. M. Abramowitz and I. A. Stegun, Handbook of mathematical functions. National Bureau of Standards, Applied Mathematics Series – 55, 1964.
35. V.K. Melnikov, On the stability of the centre for time-periodic perturbations, Trans. Moscow Math. Soc. No.12 (1963) 1-57
36. Wiggins S. Chaotic Transport in Dynamical System. Springer-Verlag. 1992.
37. P. J. Holmes, J. E. Marsden, Horseshoes and Arnold diffusion for Hamiltonian systems on Lie groups, Indiana Univ. Math. J. 32 (1983) 273-309.
38. M. Inarrea, V. Lanchares, Chaos in the reorientation process of a dual-spin spacecraft with time-dependent moments of inertia, Int. J. Bifurcation and Chaos. 10 (2000) 997-1018.
39. Jianhua Peng, Yanzhu Liu, Chaotic motion of a gyrostat with asymmetric rotor, International Journal of Non-Linear Mechanics, Volume 35, Issue 3 (2000) 431-437.
40. K.H. Shirazi, M.H. Ghaffari-Saadat, Chaotic motion in a class of asymmetrical Kelvin type gyrostat satellite, International Journal of Non-Linear Mechanics, Volume 39, Issue 5 (2004) 785-793.
41. A.V. Doroshin, Modeling of chaotic motion of gyrostats in resistant environment on the base of dynamical systems with strange attractors. Communications in Nonlinear Science and Numerical Simulation, Volume 16, Issue 8 (2011) 3188–3202.
42. L.M. Pecora, T.L. Carroll, G.A. Johnson, D.J. Mar, Fundamentals of synchronization in chaotic systems, concepts, and applications. Chaos 7 (4), 1997.
43. S. Boccaletti, J. Kurths, G. Osipov, D.L. Valladares, C.S. Zhou, The synchronization of chaotic systems. Physics Reports 366 (2002) 1–101.
44. Anishchenko V.S., Astakhov V.V., Neiman A.B., Vadivasova T.E., Schimansky-Geier L. Nonlinear Dynamics of Chaotic and Stochastic Systems. Tutorial and Modern Development. Springer-Verlag, Berlin, 2007.
45. V.V. Beletskii, M.L. Pivovarov, E.L. Starostin, Regular and chaotic motions in applied dynamics of a rigid body. Chaos 6 (2), 1996.

Attitude dynamics of the multi-spin spacecraft is considered.
Exact homoclinic and general solutions are obtained.
Chaotic and regular modes at presence of polyharmonic disturbances are examined.